Machining Process Model for Intelligent Rough Machining of Sculptured Parts

by

Sorin Ion Pop
Diploma in Engineering, Technical University of Timisoara, 1991

A Thesis Submitted in Partial Fulfillment of the
Requirements for the Degree of
MASTER OF APPLIED SCIENCE
in the
Department of Mechanical Engineering.

We accept this thesis as conforming
to the required standard

[redacted]

Dr. G. W. Vickers, Co-Supervisor (Department of Mechanical Engineering)

[redacted]

Dr. Z. Dong, Co-Supervisor (Department of Mechanical Engineering)

[redacted]

Dr. C. Bradley, Departmental Member (Department of Mechanical Engineering)

[redacted]

Dr. R. Vahldieck, External Examiner
(Department of Electrical and Computer Engineering)

Supervisor: Dr. G.W. Vickers and Dr. Z. Dong

Abstract

In recent years, the advent of new thermosetting materials (i.e. powders) and the widespread use of plastic materials has pushed forward the traditional sector of milling. Due to the vast amount of time required for producing moulds and dies, interest was manifested in reducing the machining time, of which rough machining represents an important component. This is usually proportional to the quantity of material that has to be removed. In the case of moulds and dies that quantity can be significant. One way to reduce the rough machining time is by operating the milling machine as close as possible to its maximum capacity. This thesis presents a strategy that allows the determination of such cutting data.

Based on the specific requirements of the Intelligent Rough Machining Approach, together with the formulations laid out by the Mechanistic Force Modeling Method, a cutting force model is introduced. A combination of dependency testing and surface generation procedures is employed to generate the model, which is used to plan the feed rates required to maintain a constant load on the milling machine. A clustering of the feed rates intervals is applied for reducing the total machining time, which results in time savings of up to 16 percent.

The features incorporated in the cutting force model are: *easy to customize, requires few cutting tests to develop, produces fast and accurate predictions and provisions are made for future upgrading.* Testing has shown good agreement between predictions and actual cutting data. Published values for differences between predictions and actual cutting forces range from -15.8 to 28.9 percent. Verification tests have produced values in the range -13 to 3.5 percent, which proves the quality of the concept.

Future work could include an investigation in the effect of tool wear on the magnitude of K_t and K_r and possibly an improvement in the design of the rotative dynamometer. The use of optimization techniques for clustering feed rates could provide additional reduction of the machining time.

Examiners:

[redacted]

Dr. G. W. Vickers, Co-Supervisor (Department of Mechanical Engineering)

[redacted]

Dr. Z. Dong, Co-Supervisor (Department of Mechanical Engineering)

[redacted]

Dr. C. Bradley, Departmental Member (Department of Mechanical Engineering)

[redacted]

Dr. R. Vahldieck, External Examiner

(Department of Electrical and Computer Engineering)

Table of Contents

List of Tables

List of Figures

Nomenclature

Symbol	Description
IRM	Intelligent Rough Machining
K_t	Specific cutting pressure (Pa)
K_r	Tangential/radial force ratio
F_t	Tangential component of the cutting force (N)
F_r	Radial component of the cutting force (N)
F	Cutting force (N)
d	Depth of cut (mm)
s, s_t	Feed rate (mm/rev/tooth)
ϕ	Immersion angle (rad)
F_x	Cutting force component on the X direction (N)
F_y	Cutting force component on the Y direction (N)
2D	Two dimensional
3D	Three dimensional
T	Total machining time (s)
UVic	University of Victoria
UBC	University of British Columbia
LabVIEW	Graphical program for instrumentation
MATLAB	Numerical computation and visualization software

A/D	Analog to digital conversion
VI	Virtual instrument used by LabVIEW
HSS	High Speed Steel
TiN	Titanium Nitride coating
CNC	Computer Numerical Controlled
MRR	Material Removal Rate
CSG	Constructive Solid Geometry
CAD	Computer Aided Design

Acknowledgements

I want to express my deepest gratitude to all those who along the years had encouraged me and provided either the moral or material support necessary for completing my degree.

My appreciation is mostly directed to my supervisors, Dr. G.W. Vickers and Dr. Z. Dong, who believed in me and offered advice when it was needed. People like S. Stevens and R. Katz will be remembered for their continuous help and friendship.

A warm thank you to Nick and Krista, my dearest friends.

TO MY PARENTS, WITH *LOVE*

Chapter 1

Introduction

1.1 Rough Machining of Sculptured Parts

Sculptured surfaces, unlike the surfaces created in Constructive Solid Geometry (CSG), are characterized by free-form nonanalytical contours. Their widespread application was triggered by three main factors. First, functional and aesthetic considerations, which were the result of study of new shapes, imposed this class of surfaces in different sectors of industry. Then, research in metallurgy produced materials that were easily deformed or moulded and finally, the electronic industry became capable of producing low-cost, highly reliable components. Consequently, more performant controllers, which permitted the generation of cutter paths that otherwise would have been impossible to obtain, were build.

Machining of sculptured parts is usually completed in two stages: rough machining and finish machining. While for roughing the main concern is efficiency, accuracy becomes the main priority in the finishing stage. Depending on the shape of the stock and part, sometimes as much as 90 percent of the machining time is alloted to

the roughing operation. A reduction of the machining time in this stage would mean a more efficient machining of the curved surface and, consequently, lower the costs of production. This can be accomplished either by maximization of the Material Removal Rate (MRR) and/or by an appropriate selection of cutters and cutting parameters.

The geometric representation and manipulation of curved surfaces, the Computer Numerical Controlled (CNC) tool path generation from a geometric model of curved surfaces, Computer Automated Process Planning (CAPP), adaptive process control, and simulation of CNC machining [4] were addressed by previous research.

The Intelligent Rough Machining (IRM) approach was developed at the University of Victoria by Dong, Li and Vickers to achieve minimum machining time in the production of sculptured parts. The proposed procedure relied, among others, on machining parameter optimization, which associated part and stock geometry, compared to the traditional investigation of the process-related parameters.

A further reduction of the machining time may be obtained by upgrading the IRM approach with a machining process model. This model permits the simulation of the cutting forces, so that feed rate can be planned accordingly.

1.2 Previous Research on Milling Force Modeling

The research on cutting forces during milling began as early as 1941, when Martelotti conducted an in-depth study of the chip formation [19]. Since then, a plethora of researchers have studied cutting forces dynamics.

1.2.1 Study on Cutting Forces Variation

Tlusty and MacNeil presented a study on the variation of the cutting forces in end milling for both steady cutting conditions and during the entering of the milling cutter (the transient case) [26]. They found that cutting force responds with a delay to a change in the feed rate. This delay often caused instability when an adaptive control system was used for monitoring the milling process.

The basic formulas introduced by Tlusty and MacNeil are

$$F_t = K_t \cdot b \cdot h \tag{1.1}$$

$$F_r = K_r \cdot F_t \tag{1.2}$$

$$F = \sqrt{F_t^2 + F_r^2} \tag{1.3}$$

where F_t is the tangential component of the cutting force for one tooth, F_r is the radial component of the cutting force, b is the width of cut (measured parallel to the axis of the cutter), h is the chip thickness and, K_t is a constant called specific force or specific cutting pressure. The coefficient in Equation (1.2), the tangential/radial force ratio K_r, was considered to have a constant value of 0.3. Later researchers replaced this constant with a variable coefficient for better modeling accuracy. The relationship between the chip thickness, h, and feed per tooth, s_t, is

$$h = s_t \cdot sin\phi \tag{1.4}$$

where ϕ is the immersion angle.

In order to come up with a mathematical formulation for the cutting force during the *steady state* case, the action of one tooth is considered on the unfolded surface of cut. The three successive positions (1, 2, 3) of the cutting edge are indicated in Figure 1.1. Accordingly, the whole cutting process is divided into three phases. In the first phase, A, the length of the cutting edge is increasing from 0 to the maximum width

b. In phase *B*, the length of the cutting edge remains constant, while in phase *C* the length of the cutting edge decreases. The cutting condition can be classified into two types of cutting cycles. Type I is where the ratio of cut width, *b*, to cut depth, *a*, is small, as shown in Figure 1.1a. The type II cycle, illustrated in Figure 1.1b, corresponds to a large ratio. Tlusty and MacNeil concluded that the mathematical expressions for cutting forces in the B phase of the cut are different for these two types of cutting cycles. If cutting forces are measured along two orthogonal directions, x

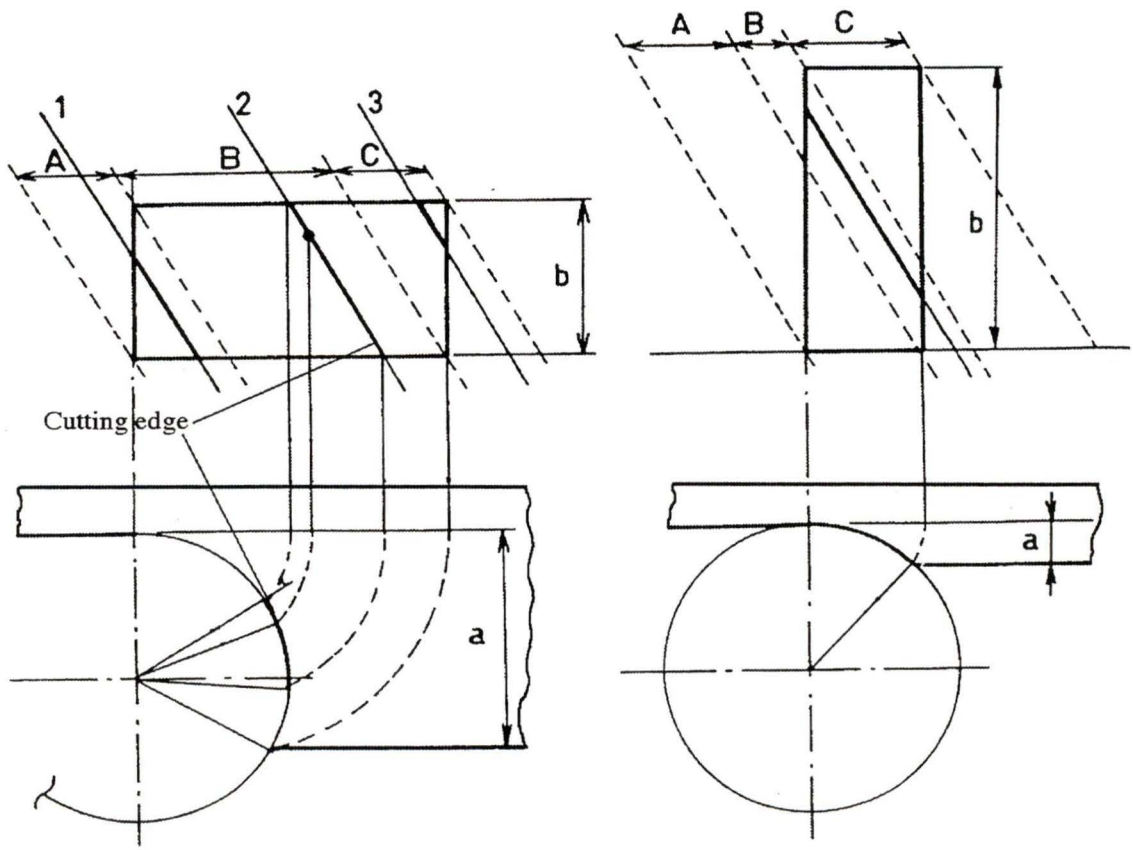

a) Type I (large a/b ratio) b) Type II (small a/b ratio)

Figure 1.1: Type I and II cutting cycles.

and y, the resultant cutting force in Equation (1.3) is

$$F = \sqrt{{F_x}^2 + {F_y}^2} \tag{1.5}$$

While Equation (1.5) is developed for a specific cutting tooth, for multiple immersed teeth, at any particular time, the equation becomes

$$F = \sqrt{(\sum_{i=1}^{n} F_{xi})^2 + (\sum_{i=1}^{n} F_{yi})^2} \tag{1.6}$$

where n is the number of flutes. One of the important observations made after determining the resultant cutting force with Equation 1.6 was that the force variation is decreasing with the increasing overlap of teeth.

The *transient case* refers to the moment when the cutter approaches the workpiece and enters the material along its normal direction. This moment can be further divided into three stages. First, due to a small depth of cut, the cutting process is similar to that described for small $\frac{a}{b}$ ratio of cut. Then, the increase of the cutting depth makes the cutting edge reach its maximum immersed length at stage two. Finally, the cutting cycle becomes similar to that exibiting large $\frac{a}{b}$ ratio of cut. For a two-fluted milling cutter, the maximum force is reached at a relatively small depth of cut, depending upon the cutter radius and width of cut. After that short distance, the milling force remains constant around its maximum value.

1.2.2 Mechanistic Force Model

Kline and DeVor developed a mechanistic force model conditioned by experimental data on average forces [29]. For down milling, the specific cutting pressure, K_t, introduced by Equation (1.2) was expressed as

$$K_t = C \cdot (f)^p \tag{1.7}$$

where C and p are constants, as defined in [24] and f is the feed rate. Another important correlation has been made between the average forces in the external $X-Y$ coordinate system and K_t and K_r.

$$\begin{aligned}
\overline{FX} &= \sum_{j=1}^{N_\theta}\sum_{i=1}^{N_z}\sum_{k=1}^{N_f}\{K_R K_T D_Z f sin[\beta(i,j,k)]cos[\beta(i,j,k)] \\
&\quad + K_T D_Z f sin^2[\beta(i,j,k)]\}/N_\theta \\
\overline{FY} &= \sum_{j=1}^{N_\theta}\sum_{i=1}^{N_z}\sum_{k=1}^{N_f}\{-K_R K_T D_Z f sin^2[\beta(i,j,k)] \\
&\quad + K_T D_Z f sin[\beta(i,j,k)]cos[\beta(i,j,k)]\}/N_\theta
\end{aligned}$$

where $\overline{FX}$ is the average X force, $\overline{FY}$ is the average Y force, N_θ is the number of angular increments, N_z is the number of axial disk elements, N_f is the number of flutes, $\beta(i,j,k)$ is the angular position of the ith disk element at the jth angular position of the cutter and the kth flute and D_z is the thickness of axial disk elements. The correlation permitted the extraction of the specific cutting pressure and tangential/radial force ratio. Kline and DeVor showed that a mechanistic force model can be employed to study the force system in detail if empirical data on average forces, from statistically designed experiments, is available. They also assumed that the wide variation of K_t suggests that it may be correlated to other variables (i.e. radial and axial depth of cut). Values larger than unity of the tangential/radial force ratio were considered to be due to improper re-sharpening. Extensive work in the study of the variation of K_t and K_r has also been conducted by Gygax [12].

Expressions for the two cutting constants, C and p, were developed. Then second order polynomial models were employed for correlating K_t and K_r to radial and axial depth of cut and feed rate

$$\begin{aligned}
K_t &= b_0 + b_1 \cdot RD + b_2 \cdot AD + b_3 \cdot f + b_1 2 \cdot RD \cdot AD \\
&\quad + b_1 3 \cdot RD \cdot f + b_2 3 \cdot AD \cdot f + b_1 1 \cdot RD^2 + b_2 2 \cdot AD^2 + b_3 3 \cdot f^2
\end{aligned}$$

where b_{ij} represent polynomial coefficients, RD is radial depth of cut, and AD is the axial depth of cut.

To demonstrate the use of the proposed mechanistic force model, Kline and DeVor studied the case of cornering cuts. The results showed that, as the axial depth of cut is varied (keeping the radial depth and feed rate constant), the relationship between average and maximum force changes considerably. Since it is the maximum cutting force that influences cutter deflection and breakage, they concluded that is important to consider this aspect of the force system. Their goal was to maintain a certain force level and to avoid potentially excessive deflections of the cutter by varying the feed rate.

1.2.3 Improved Mechanistic Force Model

A more recent study of the cutting force model for end milling was presented by Altintas and Spence [1]. In their work the force model of Kline and DeVor was integrated with a solid model of the part. An increase in the computational speed and accuracy of force prediction was achieved by reformulating the mechanistic equations into a close form. As in the case of Kline and DeVor, feed rates were scheduled during the tool path generation, thus representing an alternative to the adaptive control system. An in-depth discussion of this approach is presented in section 5.2. Tool breakage was avoided by imposing an upper limit for the maximum resultant force. A similar procedure can be applied to limit the surface roughness by simply constraining the normal force F_y through feed rate adjustment.

1.2.4 Recent Research and Developments

In recent years efforts have been made to improve the mathematical models introduced in previous research and to improve the force prediction accuracy. Some work has been carried out in investigating the influence of different cutting parameters over the specific cutting pressure, K_t, and the tangential/radial force ratio, K_r.

Armarego and Deshpande introduced three new models to increase the modeling accuracy, the *ideal, eccentricity* and *deflection models* [8]. The *ideal model* provides qualitative trends for the average forces and torques. The *eccentricity model* allows for good predictions of the average forces and torque, and the *deflection model* accounts for unfavorable cutter deflections and provides the best predictions with the sum of cutting tests performed.

Budak and Altintas increased the accuracy of calculations for milling force coefficients [7] by combining oblique geometry with orthogonal cutting data. Stabler's rule, which states that the chip flow angle is equal to the angle of obliquity, was analyzed. Resulting was a new method for more accurately estimating the chip flow angle.

Kline and DeVor, in their recent work, have quantified the effects of cutter runout [28]. Mathematical models were developed for the cutting geometry, tooth radius, chip thickness, and entry and exit angles for end milling with cutter offset or runout. The ratio of the runout to the feed rate was identified as an important parameter in identifying the effect of the runout on the cutting force.

Researchers, like Moriwaki and Shamoto, have introduced optimization techniques into their force coefficients predictions [21]. The method led to a reduction in the number of tests necessary for a given set of cutting conditions. The same group of researchers have included cutter wear into the formulation used to determine K_t and K_r.

The effect of pressure and friction acting on the cutter-chip interface and that of the cutting speed have been studied by Yucesan, Xie and Bayoumi [9].

In the recent work, carried out by Yucesan and Altintas, the effects of chip thickness, rake angle and cutting geometry on chip flow, rake face friction and pressure, and cutting forces were analyzed. A general three-dimensional mechanistic force model for peripheral milling processes was presented [10].

1.3 Research Objectives

The present work proposes to study the effectiveness of a machining process model that is to be used in conjunction with the IRM approach. A dynamometer, connected to a data acquisition system, is employed to obtain cutting force measurements from statistically designed cutting tests. A machining database is to be created from cutting data and the effects of various machining parameters are to be studied. The information contained in the database is then used for generating a machining process model, which provides predictions of the cutting force. Using the predicted values of cutting force and imposing certain physical constraints to the machining process, it is possible to determine an optimum feed rate.

1.4 Summary of Contents

The IRM approach, with its components, tool path generation and machining parameter optimization, is presented in Chapter 2. Also, included in this chapter are the reasons for seeking to develop a machine process model and the requirements imposed on such a model. To address the force measurement, Chapter 3 contains the description of the measuring device - a rotational dynamometer - and its construction,

principles of operation and calibration methodology. The signals produced by the dynamometer are picked up and stored by a data acquisition system. Its component parts and the sampling procedure are illustrated in the same chapter.

In order to assemble a machining process model from cutting data, a testing strategy was devised. Test planning details are found in Chapter 4, together with an account of the cutting force sampling procedure. Before proceeding to the actual generation of the model, data processing is required. A description of those operations is also included in Chapter 4.

In the introduction to Chapter 5, an example of the usage of the mechanistic force model in a solid modeller-based, process-simulation system is presented, followed by a review of the requirements to be satisfied by the machining process model, and a complete description of the model itself. A final assessment of the model is done, and the results are then compared to values from published data.

The implementation of the machining process model is provided in Chapter 6. A study case is presented and the conclusions drawn are then applied to a more general contour map layer. Conclusions and other observations, together with possible areas of future investigation, are grouped in the final chapter.

Chapter 2

Machining Process Modeling in Intelligent Rough Machining

2.1 Overview of the Intelligent Rough Machining Approach

A new approach to rough machining of sculptured parts, that allows minimum machining time and consequently a high productivity, was developed by Li, Dong and Vickers [4]. The Intelligent Rough Machining (IRM) of sculptured parts consists of two parts, namely: tool path pattern generation and machining parameter optimization.

2.1.1 Tool Path Generation

Contour mapping was used instead of the more common offsetting approach (Figure 2.1), so that the machining of a three-dimensional (3D) surface was transformed into

a series of two-dimensional (2D) cutting problems. Consequently, a reduction of the cutting time was obtained by avoiding the blank cuts resulting from the use of the offsetting approach. In the case of the offset approach [5], the first layer is generated

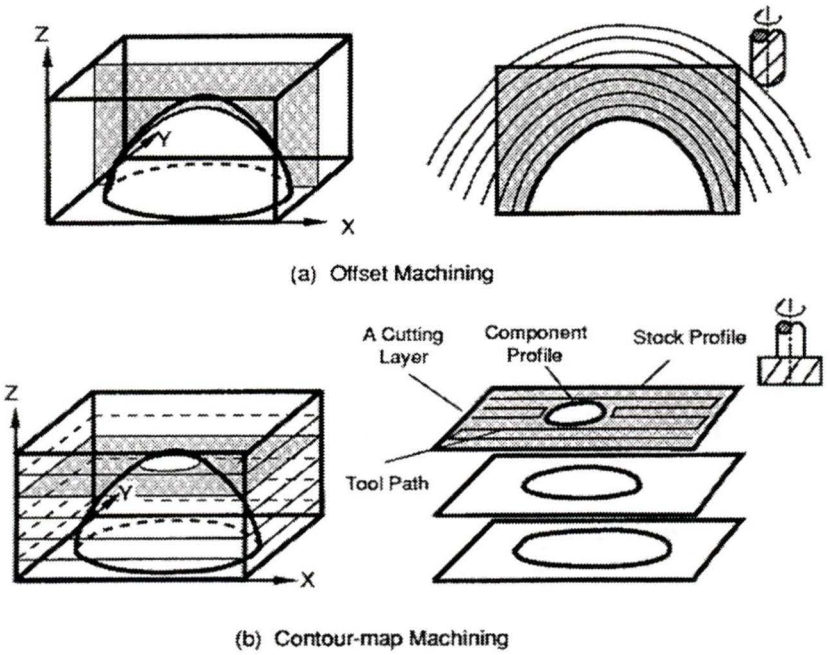

Figure 2.1: Offset and contour map machining approaches.

by offsetting the depth of cut distance from the surface of the part. Then, the second layer is obtained by repeating the process of offsetting but this time from the surface of the first layer. The whole procedure is applied until all excess material has been removed. To generate the cutting layers, the 3D normals of all surfaces, original and offsetted, have to be calculated. Usually, a ball end mill is used to machine the resultant surfaces.

When machining a sculptured part following the contour map approach, producing a 3D surface is reduced to machining parallel layers, from top to bottom. Each layer is analyzed, and a cutter path is determined such that the machining time is kept to a minimum. At the end of machining, a final cutting pass is required to remove

the gouges previously created. When the shapes of stock and part are significantly different, the offset approach results in a lot of wasted cuts. On the other hand, for machining complicated pockets or for finish cuts, the offsetting of the part is favoured.

In conclusion, contour mapping is a strategy that proves efficient for rough machining, mainly because the complex 3D problem is reduced to simpler 2D cases and a more productive cutter, an end mill, is used. A fast algorithm for generating 2D tool paths was introduced by Li, Dong and Vickers [6] and is implemented in the IRM approach. This technique reduces the amount of time required to generate the offset curves from *O(N logN)* to *O(N)*.

To deal with the 2D machining situations, various layer shapes, covering the single island, no island and multiple island cases, were investigated. Six feasible tool path patterns for the single island case are presented in Figure 2.2. For layers with no

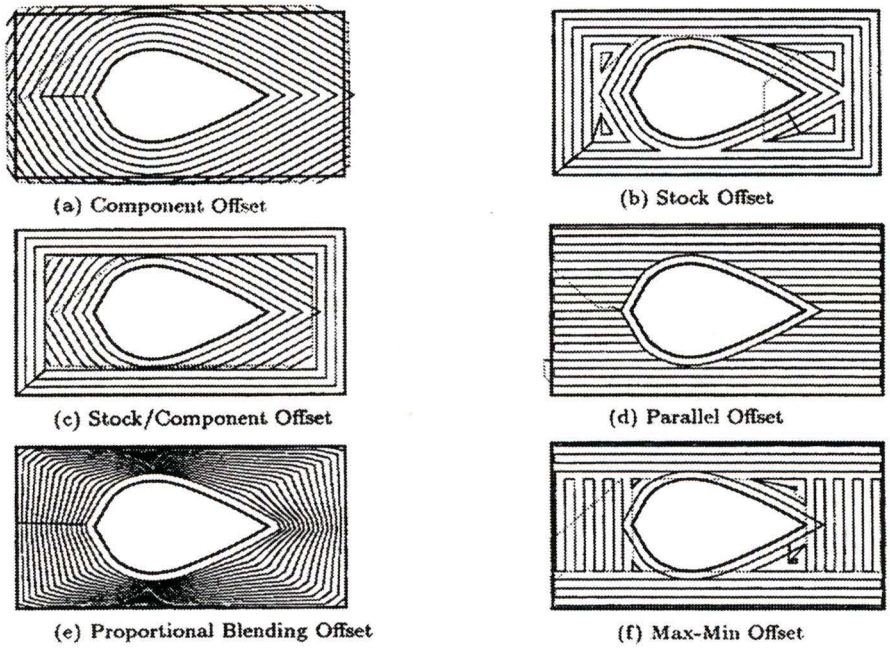

Figure 2.2: Tool path patterns for the single island case.

islands, either a parallel offset approach (when the layer is convex) or a stock offset pattern (for a nonconvex shape layer) is recommended. In the case of cutting layers with multiple islands, the same two patterns can be applied successfully. Another suitable approach is the *convex hull approximation*, which generates a convex hull containing all islands and then treats the resulting hull as a single island.

The total machining time is used as a measure to compare the suitability of the cutting patterns. Total machining time is a function of the tool path length and feed rate. The tool path length is comprised of the sum of all cutter motions, like cutting, tool plunging or retracting, and rapid traverse. In order to determine the cutting pattern that produces the shortest machining time, for a pre-determined feed rate, an investigation of all six patterns is required. A heuristic-based method has been proposed. The procedure relies on the fuzzy pattern clustering and matching principle, which states that adjacent layers may have similar shapes and therefore share a common optimal tool path pattern.

There are three main steps for identifying the optimal tool path pattern: cutting layer clustering, tool path pattern analysis and identification of the optimal pattern. The clustering of the cutting layers is based on a parametric description of the layer's shape. The center of such group is considered to define the so-called prototype layer shape, which is used to perform an analysis of the tool path patterns. After all six patterns have been investigated, the one yielding the minimum tool path length is chosen for that particular cluster.

2.1.2 Machining Parameter Optimization

The machining parameter optimization includes the study of process parameters such as feed rate, cutting speed, and depth of cut, as well as of geometry related parameters,

such as total number of cutting layers or the uneven distribution of cutting depths. The objective of the optimization is to minimize the total machining time, T, with respect to the machining parameters. The objective function is

$$T = T_c + T_m + T_u + T_d \cdot \frac{T_c}{T_l} \tag{2.1}$$

where T_c is the total cutting time, T_m represents the tool approaching and retreating time, T_u is the loading and unloading time, T_d accounts for the tool change time, and T_l is the tool life. In the case of rough machining, the last two components have much less influence than the rest of the terms, so they are ignored completely. In the general case, T_c and T_m are influenced by the number of cutting layers, N; feed rates $f_1, f_2, \ldots, f_N$ per cutting layer; depth of cut (height) of each layer $d_1, d_2, \ldots, d_N$; the geometry of sculptured surface $f(x, y, z)$ and stock $s(x, y, z)$; and tool patterns for each layer $P_1, P_2, \ldots, P_N$. So the total time, T, becomes

$$T = F(N, f_1, \ldots, f_N, d_1, \ldots, d_N, f(x, y, z), s(x, y, z), P_1, \ldots, P_N) \tag{2.2}$$

Along with the objective function, a set of physical and geometrical constraints were imposed.

Initially, the determination of cutting depth was an objective of optimization; but because of its minor influence on the total machining time, it was assumed that all depths of cut are equal, thus reducing the number of unknowns. The result of the optimization process is similar to that illustrated in Figure 2.3, where A represents the optimum number of layers, B is the total cutting time if suggestions of the machining standards are considered, and C is the time required by an adaptive controlled approach to generate the same part.

In conclusion, an improved approach to the rough machining of sculptured parts was introduced. The use of contour mapping as opposed to the offsetting technique

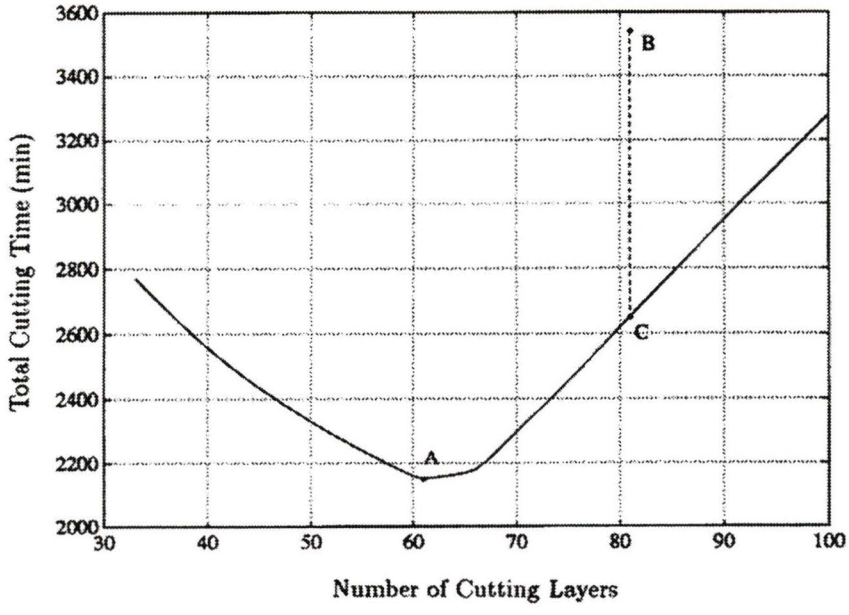

Figure 2.3: Optimum number of cutting layers.

and the optimization of the number of cutting layers resulted in a significant reduction in the total machining time.

2.2 Why a Machining Process Model?

In the optimization phase of the IRM approach, the feed rates were selected from machining standards; and they were constant throughout the machining of a layer. It was also shown that the unit cutting volume of milling is determined by feed rate, among other parameters. Consequently, a reduction of the total machining time would be possible by utilizing a variable feed rate satisfying certain physical constraints. Also, instead of working with suggested values, which in most cases are overly conservative, predictive values derived from a machining process model based on cutting tests would be more realistic. This work presents such a machining process

model and its blending in the IRM approach.

A machining process model that would be suitable for implementation in the IRM approach should satisfy the following:

- is easy to use
- has low computational costs;
- is designed for rough machining of sculptured parts (reduced number of work-piece materials and milling cutters)
- requires a small number of cutting tests to develop
- shows reasonable prediction accuracy

Based on the above features, a modified cutting force model is described in the following chapters.

Chapter 3

Design of the Cutting Force Measuring System

In order to measure the tangential and radial cutting force components, a dynamometer was built by Li [16]. The dynamometer consists of a tubular section onto which semiconductor strain gauges are bonded, as shown in Figure 3.1. The electrical signals produced by the strain gauges are collected and transmitted through slip rings and brushes to a data acquisition system. This tubular section is installed into a rotary tool holder adapter that is inserted in the milling machine's spindle. At the other end a tool adapter provides the connection between the milling cutter and the dynamometer. The dynamometer has proven [16] to be reliable for measuring tangential and radial cutting force components. However, in comparison to the commercial table-mounted dynamometer, it is more flexible and induces chatter at moderate depths of cut.

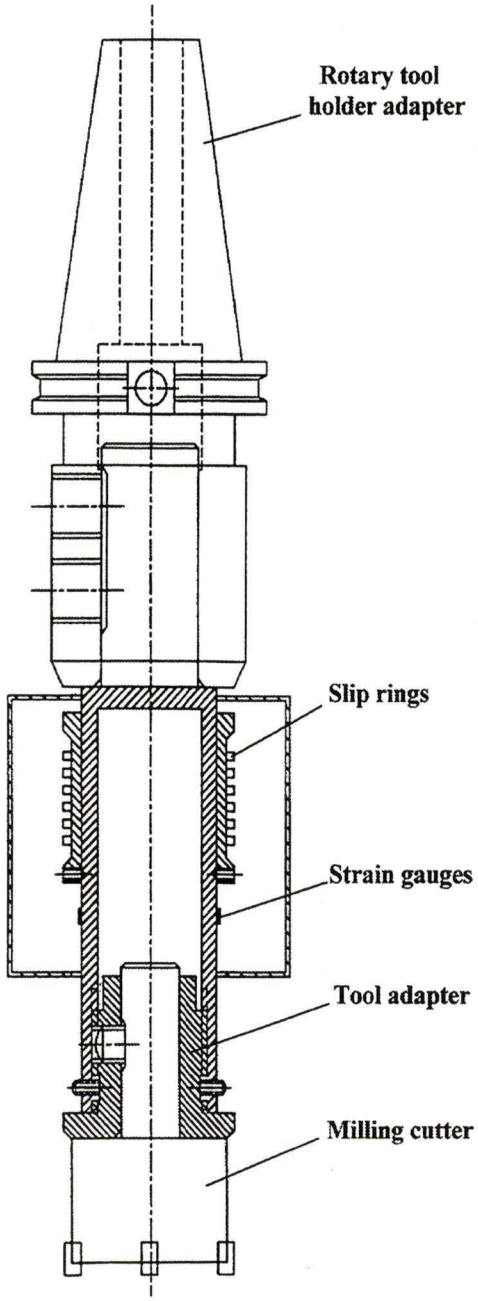

Figure 3.1: Schematic diagram of the dynamometer.

3.1 Dynamometer

3.1.1 Construction of Dynamometer

The design and construction of the dynamometer have been fully explained in [16]. Some of the features that were incorporated include:

- high sensitivity
- capable of measuring bending and/or torsional strains
- built-in temperature compensation circuitry
- high output signal/noise ratio

The main components are a tubular shaft made of steel with ultimate strength, $\sigma_u = 1GPa$, yield strength, $\sigma_y = 500MPa$, and elasticity modulus, $E = 205GPa$, three pairs of strain gauges, slip rings and their respective brushes, three half bridge circuits, and analog amplifiers and filters.

The design of the dynamometer consisted of three main stages. First, the theoretical strain gauges' output was calculated, both from bending and torsional stresses. Then, the shaft's material was chosen, its shape defined and finally, the shaft was checked for maximum shear stress and fatigue. To ensure good dynamic behaviour and measurement accuracy, the natural frequency of the assembly was calculated. Vibrations in longitudinal, transversal and torsional directions were considered.

3.1.2 Principle of Operation

The dynamometer used for measuring the tangential and radial cutting forces utilizes semiconductor strain gauges arranged in a Wheatstone half-bridge circuit. Figure

3.2 shows the positioning of the strain gauges onto the tubular shaft. Two pairs of strain gauges are orthogonally oriented, while a third pair is installed in between them forming a 90° angle. The pair labelled *Gauge 1* measures the radial component of the cutting force, while the *Gauge 2* pair is used for measuring the tangential component. Cutting torque may be measured with the third pair. The principle of measurement is illustrated in Figure 3.3. When a force, F_v, is applied at a distance, L, from the axis of the strain gauges, an electric signal, proportional to the bending strain, is produced. A Wheatstone bridge circuit was used because of its exceptional sensitivity. Ideally, the strain gauge is the only resistor in the circuit that varies due to a change in strain [22]. To read the change in resistance caused by strain on a gauge, two common methods are used. Either an indicator rebalances the bridge and displays the micro-strain required to do that, or an indicator, calibrated in micro-strain, will respond to the voltage output of the bridge. This second approach was applied in this work. The measuring circuit is shown in Figure 3.4, where 1, 2 represent the semiconductor gauges and 3, 4 are the balancing resistors.

3.1.3 The Calibration Procedure of the Dynamometer

Static Calibration

The static calibration of the dynamometer was performed on a Materials Testing System (MTS) machine, using a setup as shown in Figure 3.5. In order to reproduce the actual load conditions in cutting processes, a jig was built. This jig provided adequate fixation and support for the dynamometer. The strain gauges that measure the cutting force components were alternatively subjected to loads that varied from 0 to 600 lbs in 50 lbs increments. A multimeter was used for voltage readings. Recorded voltages were then presented in a graphical form and linearity of the output was

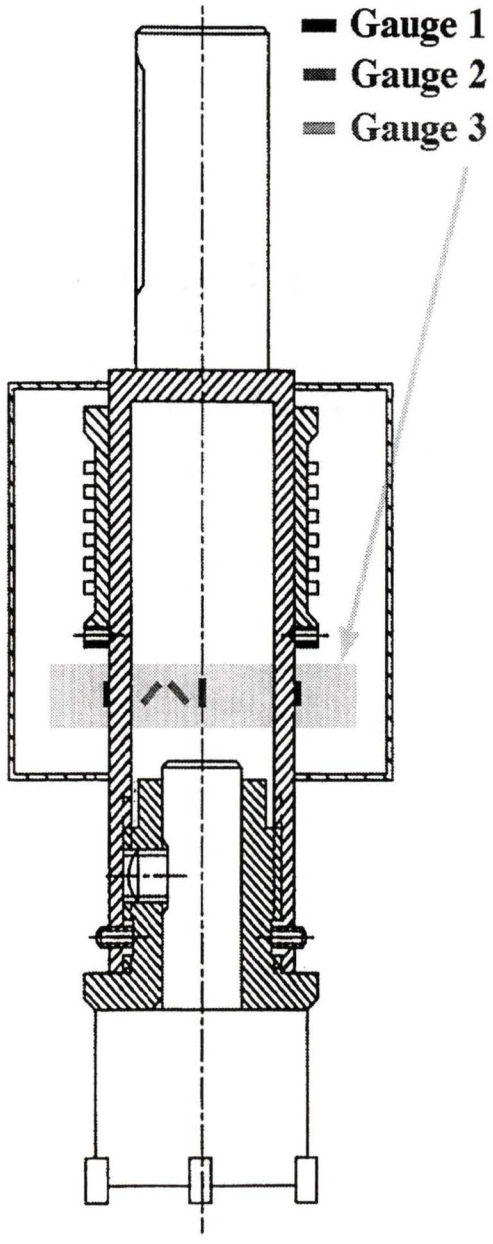

Figure 3.2: Strain gauges arrangement.

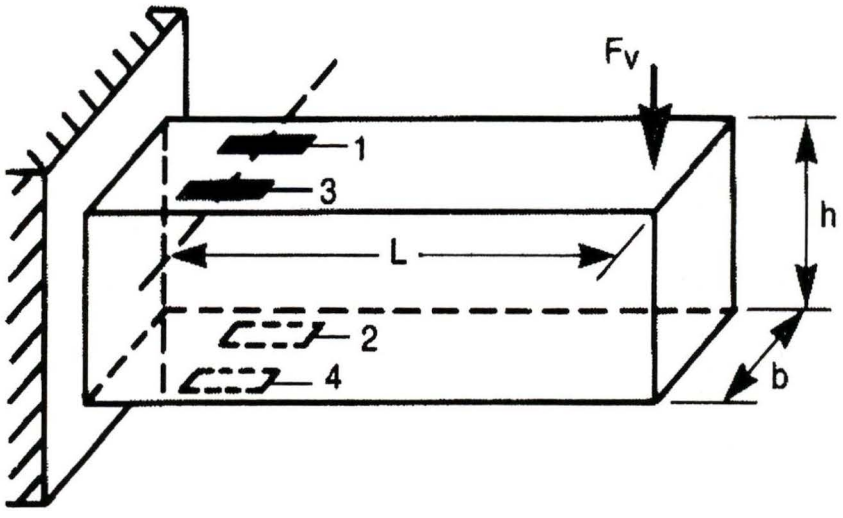

Figure 3.3: Principle of operation for strain gauge measurement.

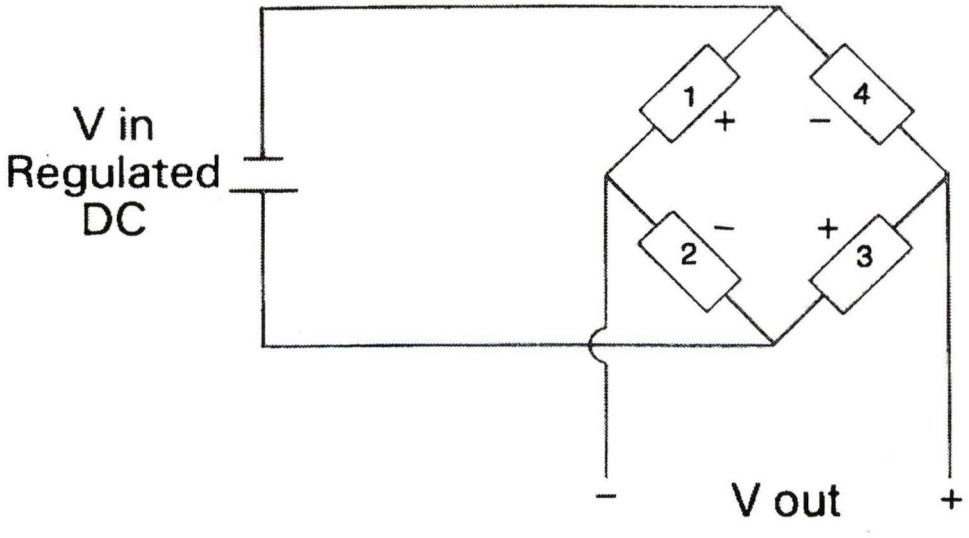

Figure 3.4: Wheatstone bridge circuit.

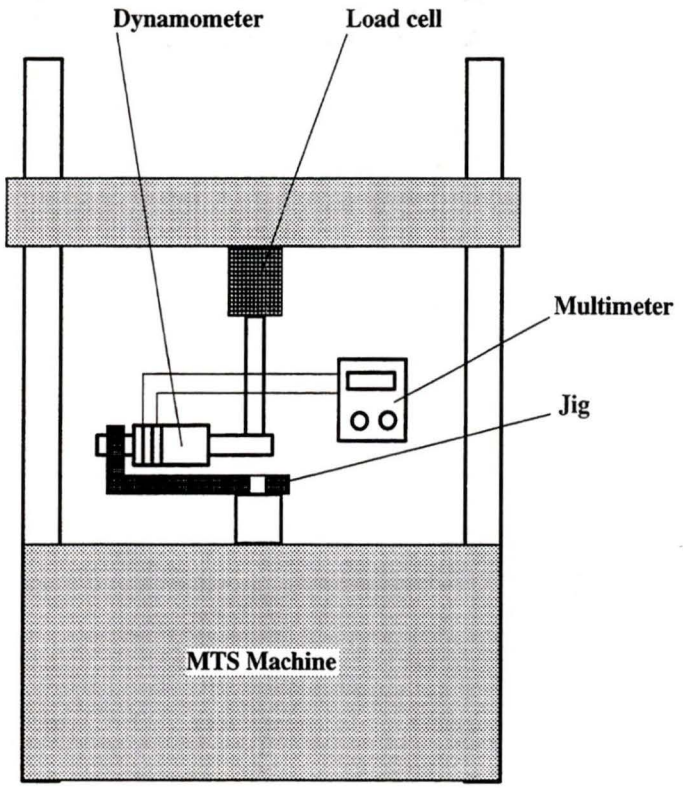

Figure 3.5: Static calibration setup.

checked. At this stage of the calibration, it was observed that the unloaded pair of strain gauges produced a low output signal. This parasitic signal was considered to be due to some misalignment of the strain gauges during installation. In order to compensate for this misalignment, a decomposition matrix was determined.

Verification of the Static Calibration

Testing of the dynamometer was previously carried out by Li [16]. He checked the following

- *linearity* of the strain gauges' output. It was found that the mean square errors for the linear fitting of the calibration data are 0.0013 (V_x/F_x), 0.00067 (V_y/F_y) and 0.00077 (V_t/F_x). V_x, V_y and V_t represent the voltage output of strain gauges.
- *repeatability.* Tests have shown that changes in the slope of linear fitting are less than 0.0001 V/lbs.
- *creep.* Under the constant load of 200 lbs, the measured creep was 2.2 mV over a period of 3 minutes. The relative error was 0.3 percent.
- *hysteresis.* When load was slowly increased from 0 to 600 lbs and then gradually removed, the measured hysteresis was 0.0192 V.
- *temperature sensitivity.* The effect of temperature changes over the strain gauges' output was minor.

As a means of assessing this calibration against a known commercial unit, a set of tests was conducted using the dynamometer provided by Altintas (UBC). Each test targeted specific areas, such as re-calibration of the dynamometer, verification of the measuring device in cutting tests and determination of the natural frequency. To

re-calibrate the dynamometer, a setup similar to the one illustrated in Figure 3.6 was used. The dynamometer built at UVic was installed in the milling machine's spindle,

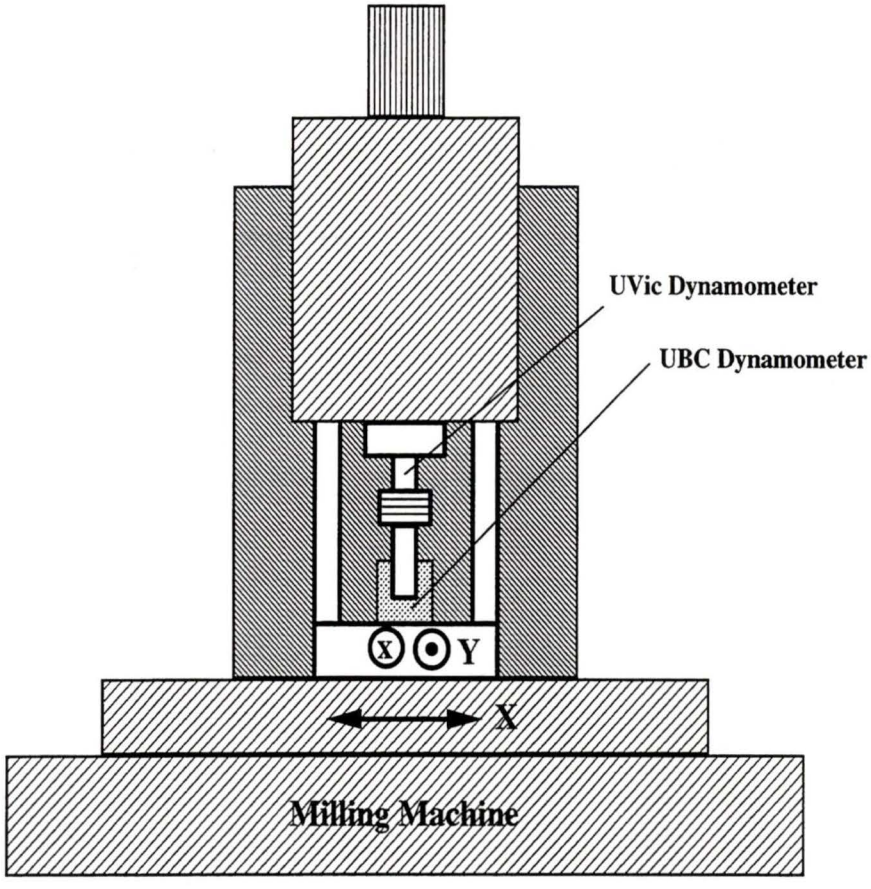

Figure 3.6: Experimental setup for the static load test.

while the off-the-shelf measuring instrument was fixed on the machine's table. A manual orientation of the UVic dynamometer, for aligning each pair of strain gauges to the compression load created by the relative movement of the two dynamometers, was executed. During the re-calibration test, the controlled parameter was the displacement of the table, which was varied in small steps from 0 to 1 mm. After each increment, voltage readings were taken from both dynamometers. The voltage readings were converted through the decomposition matrix and sensitivity factor,

respectively; and the results were expressed in force units. The test data given in Figures 3.7 and 3.8 show that, while both dynamometers exibit a linear output, they are inconsistent in magnitude. A new and improved method of calibration was adopted and proven to solve this inconsistency. In the second phase of the joint testing with

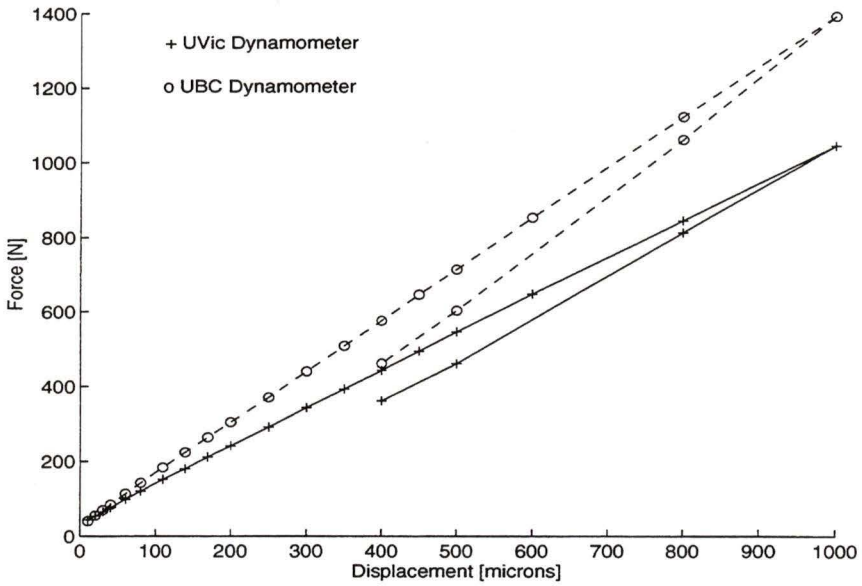

Figure 3.7: Relationship between displacement and output voltage - X direction.

UBC, the same arrangement of the measuring devices was employed for a total of 11 cutting tests. Knowing about the discrepancy between the two dynamometers, cutting forces were calculated only from the output of the off-the-shelf dynamometer. A few observations about the level of chatter reached during testing were made.

A last test determined the first natural frequency of the UVic dynamometer in two orthogonal planes. The cell was impacted with a hammer connected to a Hewlett-Packard frequency analyzer. The frequency response was measured and recorded in a file for further processing. Resultant natural frequency obtained are grouped in Table 3.1, where X and Y are the same as in Figure 3.6 and gauge 1, 2 represent the two pairs of strain gauges.

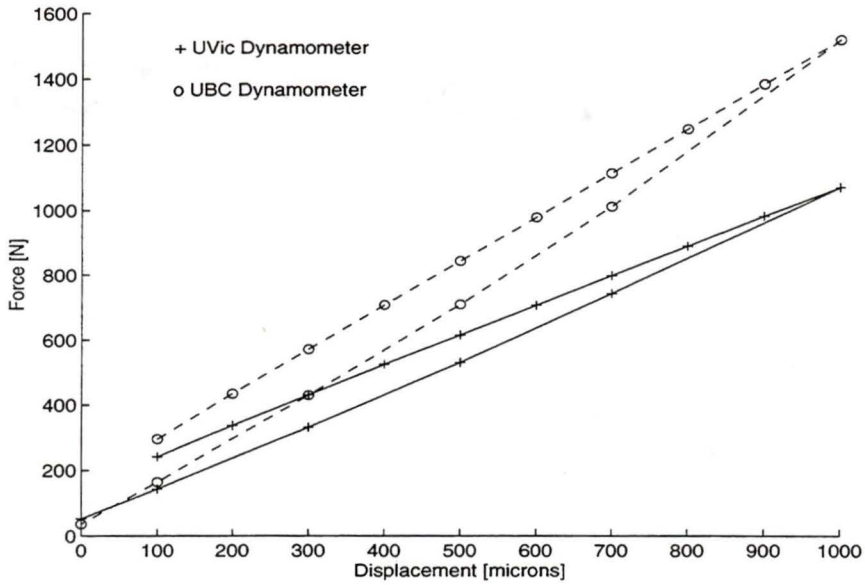

Figure 3.8: Relationship between displacement and output voltage - Y direction.

Orientation	**Direction of impact**	**Natural frequency (Hz)**
X	gauge 1	318.9
X	gauge 2	347.4
Y	gauge 1	294.9
Y	gauge 2	314.9

Table 3.1: Natural frequencies of the UVic dynamometer.

Dynamic Calibration

To solve the inconsistency problem encountered after the static loading of the dynamometer, a dynamic calibration was planned. The improved calibration setup is illustrated in Figure 3.9. A constant load was applied to the rotating dynamometer

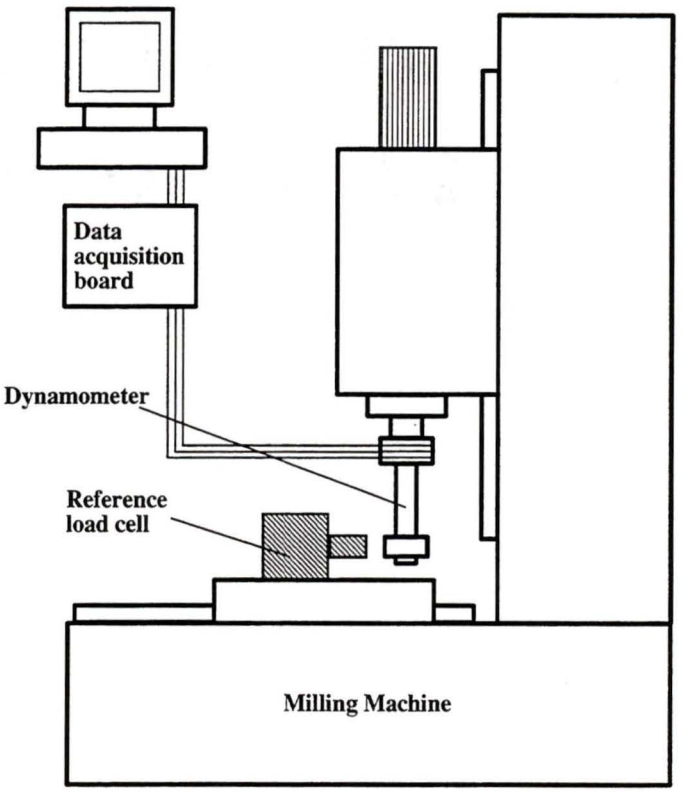

Figure 3.9: Dynamometer's dynamic calibration setup.

through a ball bearing, which eliminated the friction between the reference load cell and the dynamometer. The load was increased in increments of 25 lbs, from 50 to 300 lbs. LabVIEW was used to acquire the output of the strain gauges and plots like the one shown in Figure 3.10 were obtained. Since the magnitude of the output signal from the two pairs of strain gauges is different, two sensitivity factors have to be calculated. Figures 3.11 and 3.12 show the relationship between the applied load and the output signal. A line was fitted through the data points, thus producing a

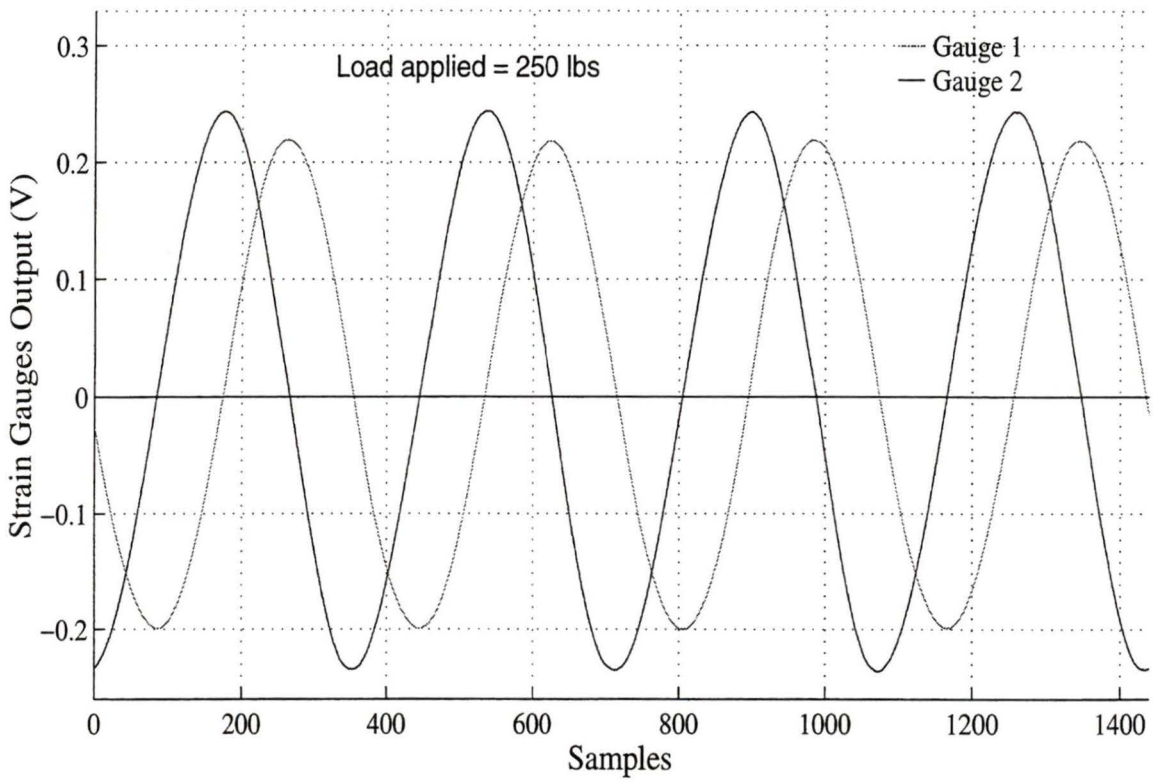

Figure 3.10: A sample plot used for the calculation of the dynamometer's sensitivity.

mathematical correlation between load and strain gauges' output. Using the sensi-

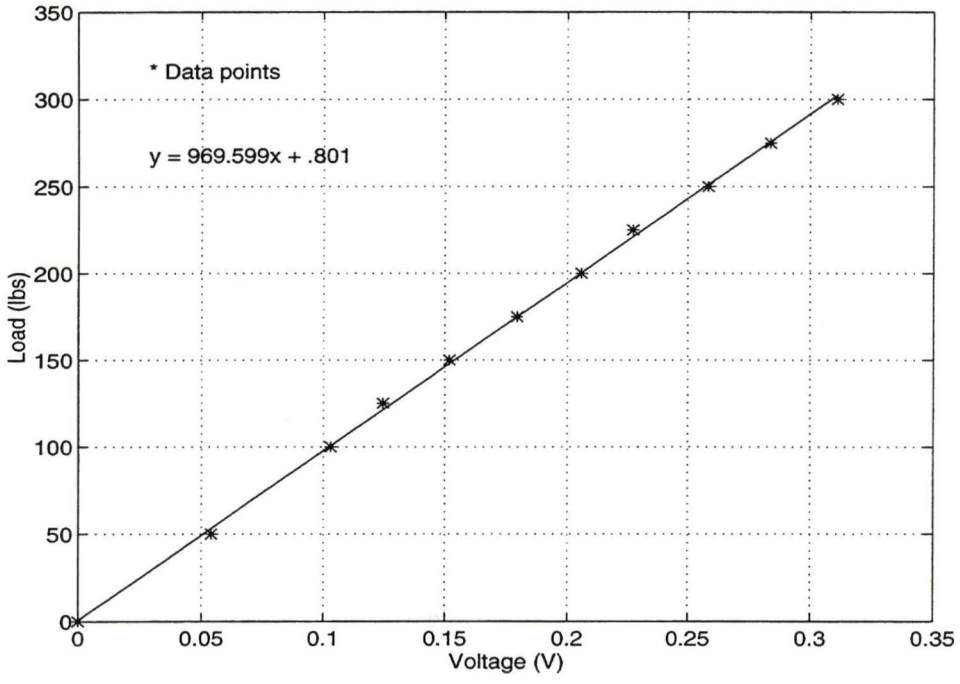

Figure 3.11: Load versus output signal for the first pair of strain gauges.

tivity calibration constant, the output voltages obtained during the joint testing with UBC were transformed into force. The effect of this conversion is illustrated in Figure 3.13. Analyzing the cited figure, it was obvious that the dynamic calibration gives satisfaction; and concurrently, confidence was gained in the dynamometer's operation.

3.2 Data Acquisition System

3.2.1 Overview

The data acquisition system for force measurement was based on the LabVIEW Lab-NB Multifunction 12-Bit A/D Board. The computer that provided the platform for

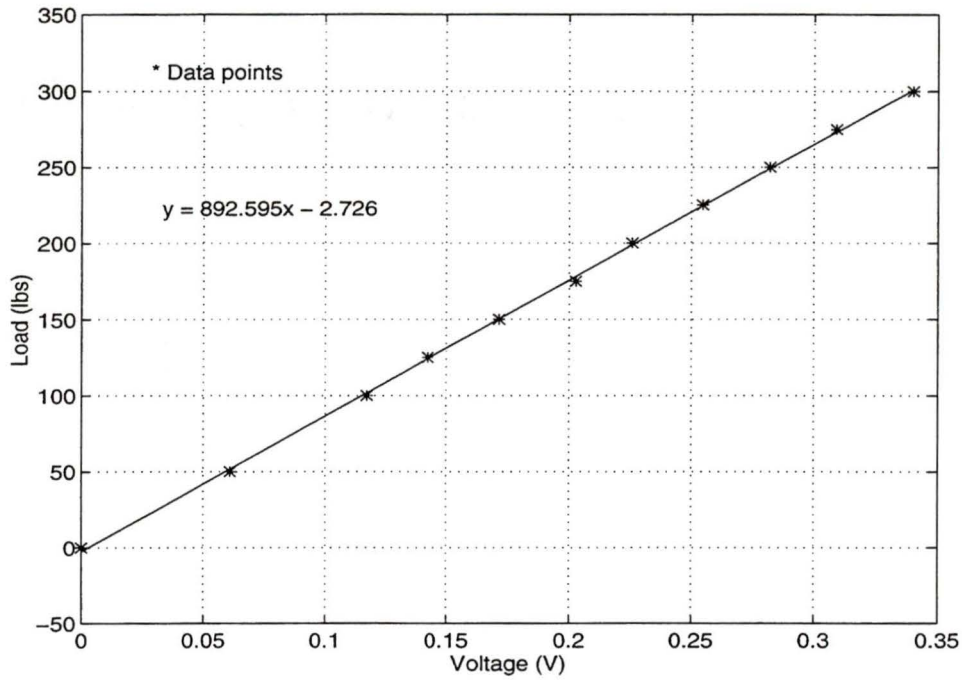

Figure 3.12: Load versus output signal for the second pair of strain gauges.

the LabVIEW Card was an Apple Macintosh II vx with 8 MB RAM. Some of the technical specifications for the Lab-NB Board [15] are:

- number of channels 8
- analog-digital converter resolution 12-bit
- programmable gains 7 (1, 2, 5, 10, 20, 50 and 100)
- input ranges 2
  - 0 to +10 V (unipolar and gain set to 1)
  - -5 V to +5 V (bipolar and gain set to 1)
- maximum sampling rate 62.5 ksamples/sec

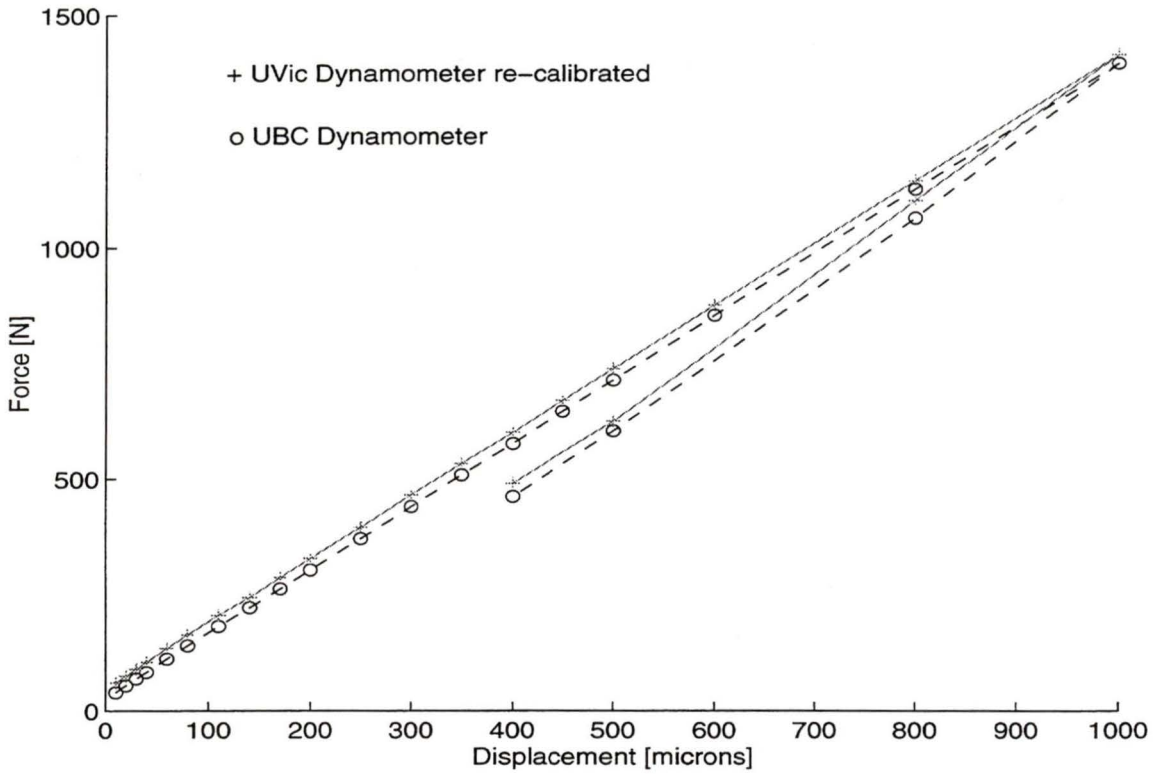

Figure 3.13: Result of the dynamic re-calibration.

This type of board permits data acquisition in either single-channel data acquisition or multiple-channel scanned data acquisition mode. Single-channel data acquisition involves selecting a single analog input multiplexer and gain setting. In multiple-channel scanned data acquisition, a set of analog input channels is scanned with a single gain setting in a round-robin mode.

A schematic diagram of the data acquisition system is presented in Figure 3.14. It should be noted that even though the system allows for a maximum of three channels to be scanned at one time, present research required only two independent channels. The third one may be connected to the data acquisition board anytime, and samples acquired from the torque channel, too. A fourth auxiliary channel was necessary to collect data from the triggering device, which was required for launching the sampling process.

3.2.2 Virtual Instrument

The application programs created in LabVIEW are called virtual instruments and referred to as VIs. A VI called by another VI is seen as a subroutine, and it is labelled subVI. The way in which such a call is made is through the icon/connector representation. The VIs have three main parts: the *block diagram*, the *front panel* and the *icon/connector*. The *block diagram* is a VI's source code (created using a graphical programming language called G); the *front panel* is the user's interface to a VI; the *icon* is the representation of the VI, and the *connector* acts as a port through which data passses from diagram to VI.

The **block diagram** of the application program used for data acquisition can be divided into three main sections: file name generation, thermal shift compensation and data acquisition.

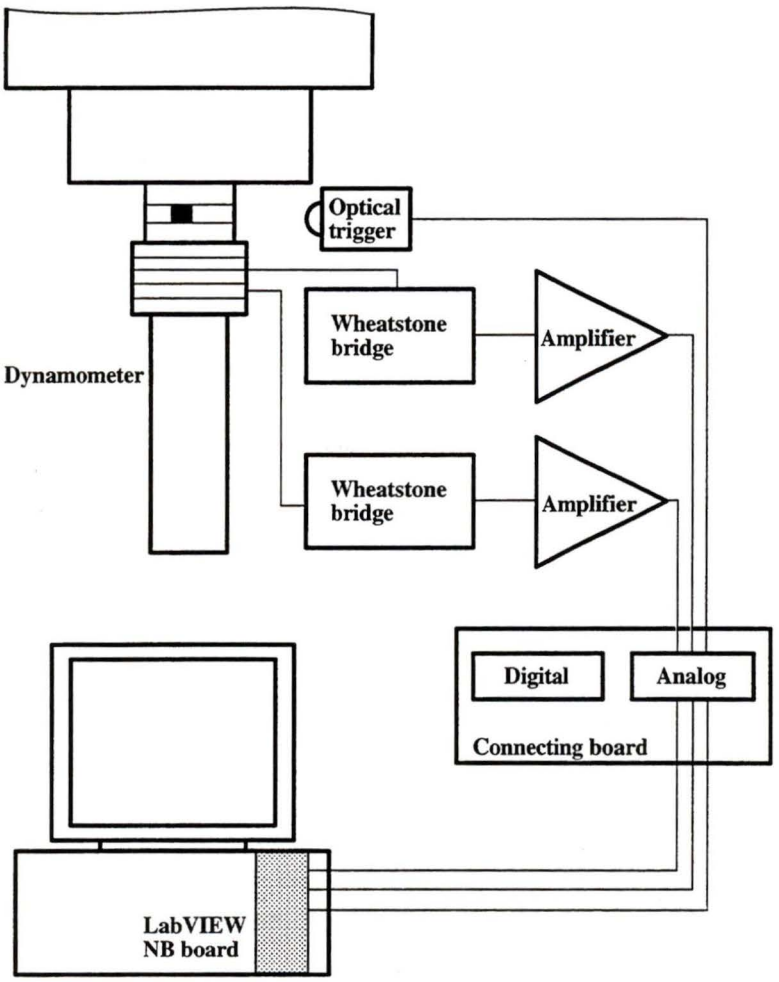

Figure 3.14: Data acquisition system layout.

In the first section, a specific file name is created. The information stored is dependent on the cutting conditions and is passed in this way to the post-processing module. For example, one of the file names generated in this section might be

mc1_al_s754d2f151e0x180_1

An explanation of the fields follows:

- *mc1* is the name of the milling cutter. Later on this symbolic name will be used for accessing information about the milling cutter.
- *al* represents the part's material; in this case Aluminum. Other materials are available for selection.
- *s754* contains the spindle speed expressed in rotations per minute. *s* is a delimiter and marks the beginning of this field, while *754* is the actual speed. The same notation system is used throughout the next four fields.
- *d2* stores the cutting depth (in milimeters).
- *f151* contains the feed rate (in mm/min).
- *e0* is the entry angle (in degrees).
- *x180* represents the exit angle (in degrees).
- *1* index that allows to differentiate among tests that have the same cutting parameters.

There are two ways to *compensate for the thermal shift*, either by taking advantage of the specialized built-in compensatory circuitry or by doing an automatic compensation. Due to its simplicity and high accuracy, the second method was preferred. A

number of 360 samples per channel were collected before the actual machining and averaged. Those average values represented the offsets and were subtracted from the dynamometer's outputs.

In the third, and most complex section, data acquisition during the cutting tests is performed. The basic component is the Lab_SCAN_Op VI [15, pp. 6-24...6-26], which performs a multiple-channel scanned data acquisition operation. Lab_SCAN_Op was included in the *mscan* subVI, which has its structure shown in Figure 3.15. After

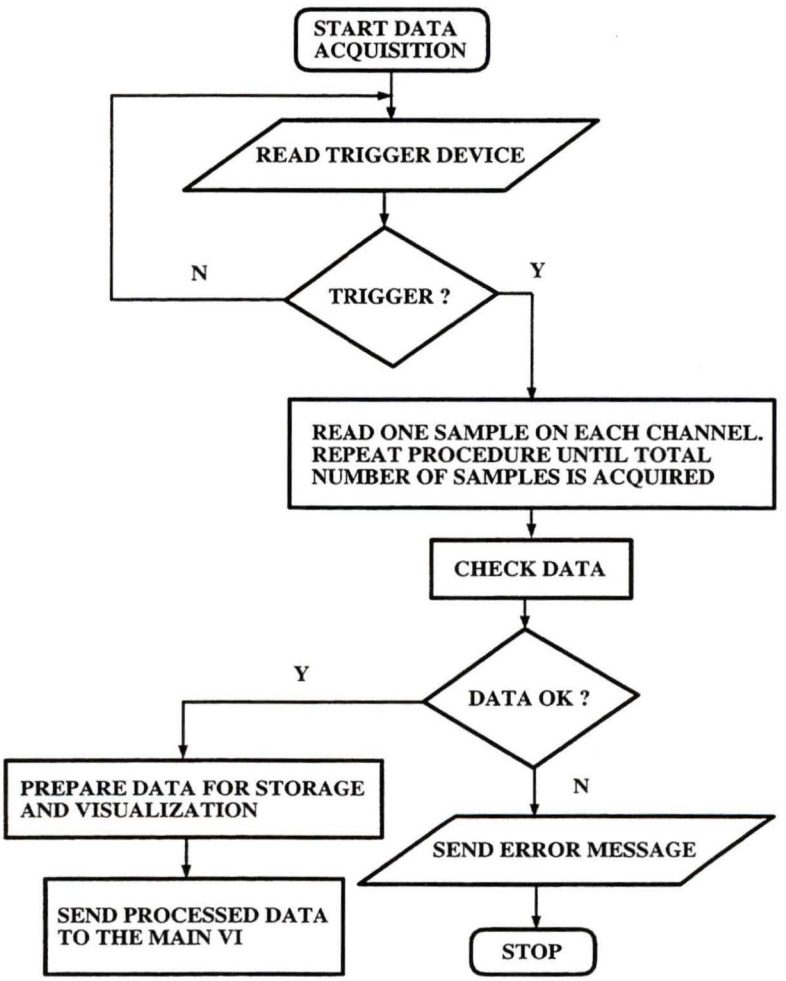

Figure 3.15: Scanning operation flowchart.

the collection of samples is finished without errors, an array containing the number

of samples/rotation/channel, the number of rotations that were inspected and the cutting data is created and saved in a file that had its name generated in the first section.

The **front panel** is the interface of the VI and represents the means through which the user is interacting with the application program. Allowable inputs are: name of the tool, depth of cut (mm), feed rate (mm/min), spindle speed (rpm), cross feed (mm), trailing angle (degrees), table feed direction (X or Y), part's material, test number, number of sampled channels and number of samples per channel. A total of three logic switches is available, for selection of the triggering method (manual or automatic), initiation of one rotation data sampling for thermal compensation and start of data acquisition. To enable quick decisions regarding the continuation of data acquisition, the results of the sampling process are visualized in a graphic window. A printout of the front panel is included in Appendix A.

Chapter 4

Experimental Procedures and Data Processing

4.1 Experimental Procedure

A total of twenty six sets of tests were conducted. Their objectives included:

- determine the influence of each cutting parameter over the cutting force, F, specific cutting pressure coefficient, K_t, and tangential/radial force ratio, K_r
- verify the dynamometer in a series of tests
- check the cutting force formulations presented in [2]
- collect cutting data that could be used to define a modified cutting force model for implementation in the IRM

Aluminum 6061-T6 was chosen for the part material due to its good machinability characteristics.

4.1.1 Variables Considered

The parameters inspected in these machining tests are feed rate, cutting speed, depth of cut, entry angle, exit angle and type of milling cutter. The initial ranges for the cutting speed, depth of cut, and feed rate were selected based on machining standards, [25], [18] and [27], suggestions. The indicated cutting data varied largely, for example, cutting speed for High Speed Steel (HSS) cutters from 30 to 60 m/min up to 100 to 150 m/min. Cutting experiments were carried out in order to determine those cutting parameters that produced the least chatter. The chosen values were:

- cutting speed: 30 to 60 m/min
- feed rate: 0.19 to 0.64 mm/tooth/rev
- depth of cut: 0.5 to 7 mm
- entry angle: 0 to 90 degrees, and
- exit angle: 120, 160 and 180 degrees

A Niagara 3/4" 2 fluted HSS milling cutter was used for all cutting tests. Geometrical characteristics of this tool include: shank diameter of 3/4", length of cut $1 - 5/16$", overall length $3 - 9/16$", and Titanium Nitride (TiN) coating. Other cutters were peripherally examined but not included in the test results. Also, different milling operations, such as climb (down) and conventional (up) milling, slotting and contour milling, were investigated. A copy of the tests performed is included in Appendix B.

4.1.2 Testing Methodology

Measurement acccuracy and repeatability were the main concerns throughout the experimentation stage. A precise and thorough testing procedure was developed and

updated to reflect the observations made during machining.

As seen, the dynamometer plays the dual role of measuring device and tool holder. Derived from its duality, careful maintenance and stringent installation requirements were imposed. Due to the electronic circuitry, which is attached to the tubular shaft, precautions were taken when cutting fluids were directed in the area of machining. Even though the electronics involved have proven quite reliable, exposed components were sometimes subjected to overloads, mainly because of difficulties in the brushes-slip rings alignment. A plastic cover was provided for the circuitry's protection; but regular adjustments of the dynamometer necessitated easy access, so the cover was removed. Regarding the milling cutter installation, the main concern was keeping the radial and axial runout below .001". The various degrees of freedom that the dynamometer allowed permitted an accurate installation. Burrs or craters, once detected, determined the replacement of the tool. Maintenance operations for the dynamometer assembly included regular cleaning of the electrical contacts and visual inspections of the milling cutter. Special attention was paid to the orientation of the cutting edges with respect to the zero point. Ideally the angle between the two is zero degrees but that proved impossible to realize. Consequently, the actual angle was measured through cutting tests; and force measurements were then shifted accordingly.

The preparation of the workpiece involved, either a new block of material to be fixed into the machine's vice or a re-positioning of the existing one. To ensure its flatness, a facing operation was performed. Before the test's cutting data was downloaded into the CNC's controller, MTI probes were used to accurately determine the origin of the coordinate system.

Parameters, required by the data acquisition system, were extracted from the testing plan and their values introduced in the VI's front panel. A short application

program was downloaded into the milling machine's controller and run simultaneously with the data acquisition VI. Initialization of the data sampling was commanded only after the cutter passed the entry stage, and the cutting force reached its maximum. A general purpose coolant was sprayed in the region of machining and chips generated in the milling process were readily evacuated from the area. Force measurements were visualized, in real time, on the VI's front panel, allowing for a quick decision regarding the continuation of the test.

4.2 Data Processing

The data acquisition system furnishes force measurements to the data processing module. The collected samples are transferred into the MATLAB environment and further processed. K_t and K_r, as well as the trends of variation for these coefficients, are determined.

4.2.1 About the MATLAB Environment

MATLAB was chosen for its unique features, described in the following quotation [20].

> MATLAB integrates numerical analysis, matrix computation, signal processing, and graphics in an easy-to-use environment where problems and their solutions are expressed just as they are written mathematically ...
>
> MATLAB is used for research and to solve practical engineering and mathematical problems. Typical uses include general purpose numeric computation, algorithm prototyping, and special purpose problem solving with matrix formulations that arise in disciplines such as automatic control theory, statistics, and digital signal processing ...

Four major categories of application programs were developed in MATLAB for:

1. plotting and digital filtering of sampled data.
2. creating a data base containing average values for K_t, K_r, F_t and F_r.
3. producing plots that correlate the changes in the cutting parameters (e.g. feed rate) to the variation of K_t, K_r, F_t and F_r.
4. combining previous results in charts describing the complex variation of K_t, K_r, F_t and F_r under the influence of two or more cutting parameters.

4.2.2 Digital Filtering of the Force Measurements

Clean signals are preferred for extracting K_t and K_r from cutting force measurements. After a number of initial tests showed the occurrence of chatter in most cases, digital filtering of the original output of the strain gauges was considered. To assist in selecting a suitable digital filter, the power spectral density and the cross spectrum of the gauges' output signals were determined. Power spectrum diagrams were plotted for two cases, first when the dynamometer is rotating but is unloaded, and second for the regular machining case. By producing the spectrum diagram for the unloaded dynamometer, it was posssible to measure the influence of the background noise. The second type of diagram permitted the determination of the first harmonics. Unfortunately, no additional information about the oscillatory motion was derived from the cross spectrum of the two force signals.

Comparing the first harmonic to the natural frequencies found in Table 3.1, a correspondence was observed. Since the energy level of the other harmonics was 10^2 to 10^3 times less than that of the first harmonic, they were discarded. An example of power spectral density diagram is shown in Figure 4.1.

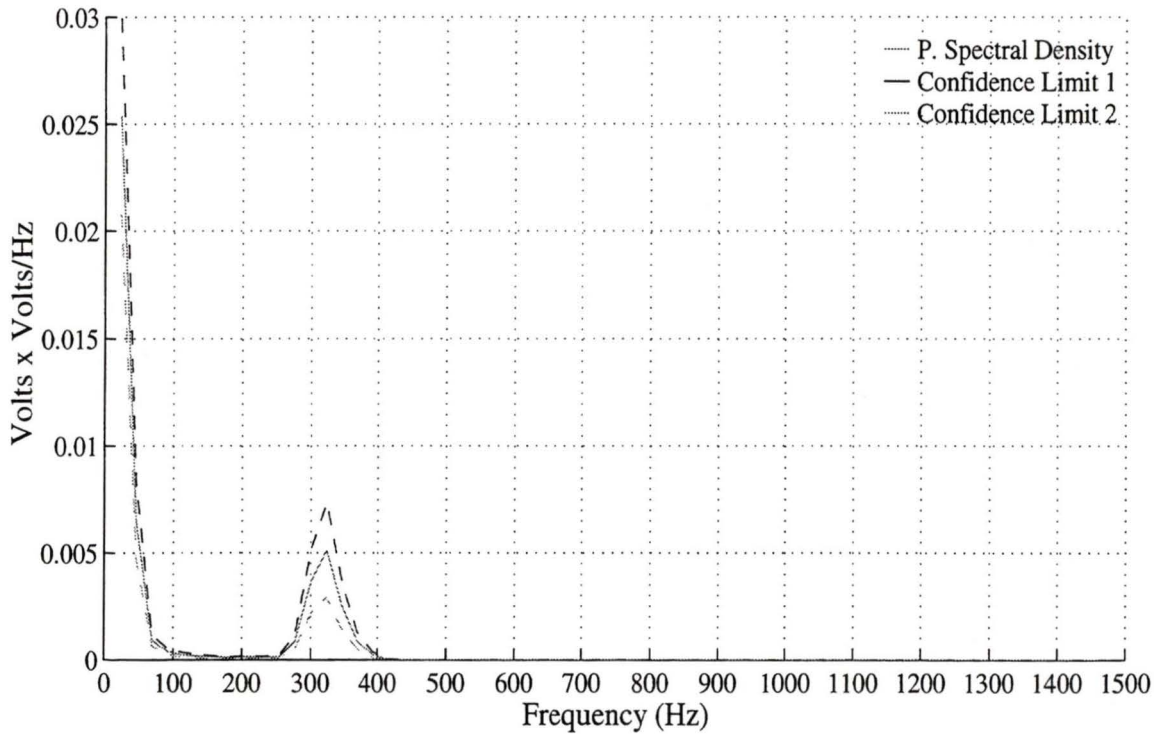

Figure 4.1: Typical example of a power spectral diagram.

Two types of digital filters were considered, a lowpass Cebyshev type II and a lowpass Butterworth filter. Using similar filter parameters, both filters behaved quite similar for full width machining, but a better fit was obtained with the first type when dealing with interrupted cuts. Consequently, the Cebyshev type II filter was selected. Experimentation with the filter's parameters pointed out values that provided very good fits. The investigated parameters and their values are the order of filter, n, 4, cutoff frequency, Wn, 200 Hz, and stopband attenuation, r, 20 dB.

The original signals were filtered in both directions (forward and reverse), thereby eliminating all phase distortions. In the same time, the applied filtering function [17] took care of minimizing the filter startup transients. Filtering the force signals for full width machining presented no problems. In the case of interrupted machining, the filtered signal was composed of an initial zero magnitude segment, with a length depending on the radial depth of cut. Appended to this segment was a second one, which was the result of the digital filtration of the force signal. This technique was applied an integer number of times, and the result is illustrated in Figure 4.2. Other methods for calculating a digital filter, such as the forward linear prediction [13], were inspected. Even though the filter's accuracy might have been improved, the computational cost incurred would have been unacceptable.

Based on the setup in Figure 3.9, an induced vibratory movement test was carried out. The scope of that particular test was to examine the influence of chatter over the cutting force magnitude. Essentially, it consisted of a rotational constant load and a superimposed oscillation with a frequency equal to that of the dynamometer's natural frequency. The oscillation was generated by a vibration exciter type 4809 supplied by Brüel-Kjær, which exerted a maximum force of 44.5 N. The transfer of vibratory energy was done through a threaded rod in contact with the ball bearing installed in the dynamometer. Due to the low force output of the shaker, the test

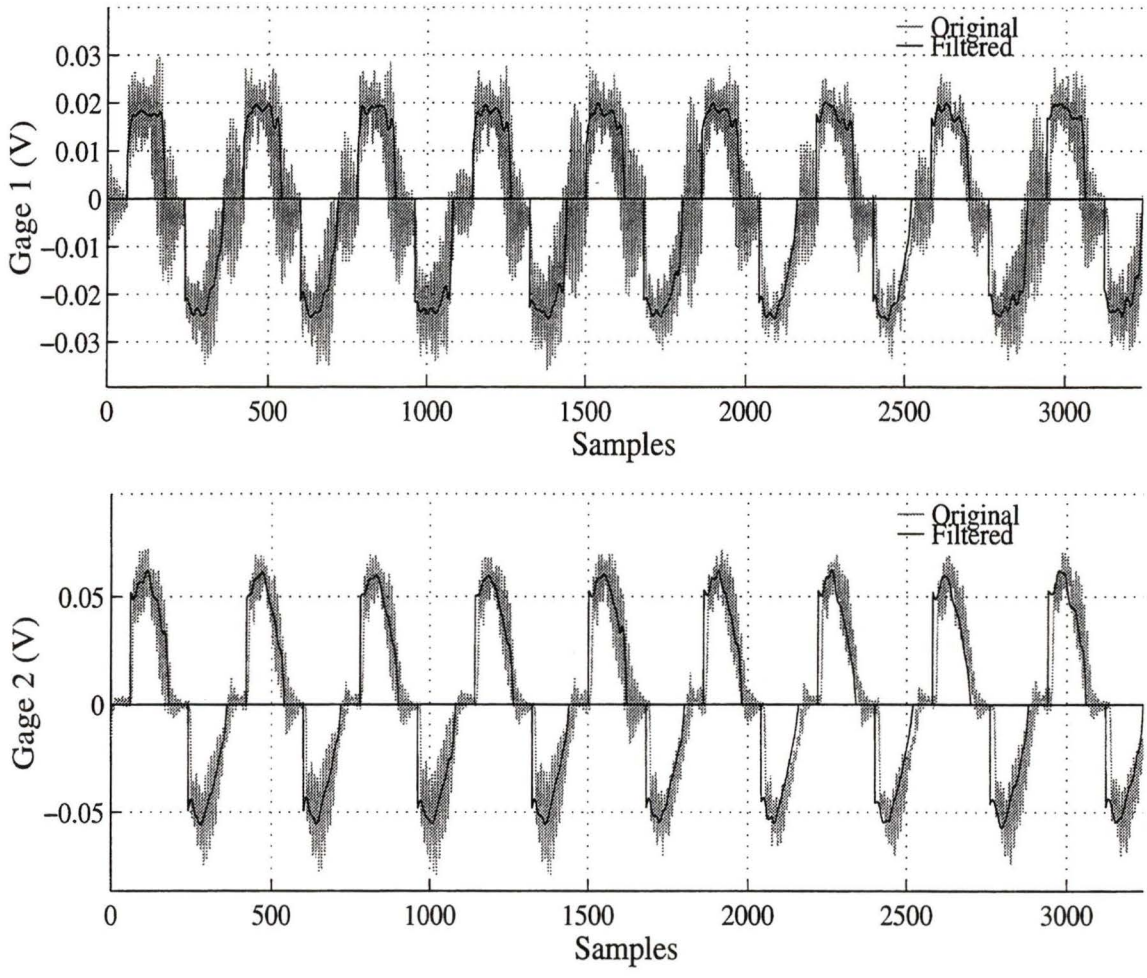

Figure 4.2: Filtration technique for the interrupted cutting case.

was not conclusive.

4.2.3 Determination of Force per Tooth

The calculation of force per tooth is used to determine the loading on each tooth for milling cutters with more than two flutes. The procedure involves the determination of the effect of the immersed teeth on the direction of the strain gauges. Knowing that the summation of those force components equals the output signal on each channel, by applying a decomposition matrix, dependent on the immersion angle of each tooth, the total load is divided among the teeth. The resulting load plots are valuable in showing the effect of toolwear over the magnitude of cutting force components.

4.2.4 Calculation of Specific Cutting Pressure and Tangential/Radial Force Ratio

After creating an extensive database of sampled data, determining the specific cutting pressure, K_t, and the tangential/radial force ratio, K_r, is solved by applying the formulas given in [2]

$$F_t = K_t \cdot d \cdot s \cdot \sin\phi \tag{4.1}$$

$$F_r = K_r \cdot F_t \tag{4.2}$$

where F_t and F_r are the values of the measured forces, d represents the depth of cut in millimiters, s is the feed rate in millimiters per tooth per revolution, and ϕ equals the angular position of the active tooth.

Averages of K_t, K_r, F_t, and F_r are stored in a database for further comparative studies. Also the information contained in the database was used to generate the skeleton lines to be incorporated in the modified cutting force model.

Chapter 5

Machining Process Model Based upon Miling Tests

5.1 The Mechanistic Force Model in a Solid Modeller Based Process Simulation System

Altintas and Spence proposed a constructive solid geometry based process simulation system for $2\frac{1}{2}$ axes milling [2]. The resultant cutting process simulator can be used to assist the planning process and online monitoring. The cutter paths are generated from a given part model, and the immersion intervals are calculated. Milling mechanics equations are used to simulate the milling process. Two options are available, either the cutting forces, torque and part dimensional errors can be predicted or the cutting parameters can be planned along the cutter paths. The structure of the system is illustrated in Figure 5.1.

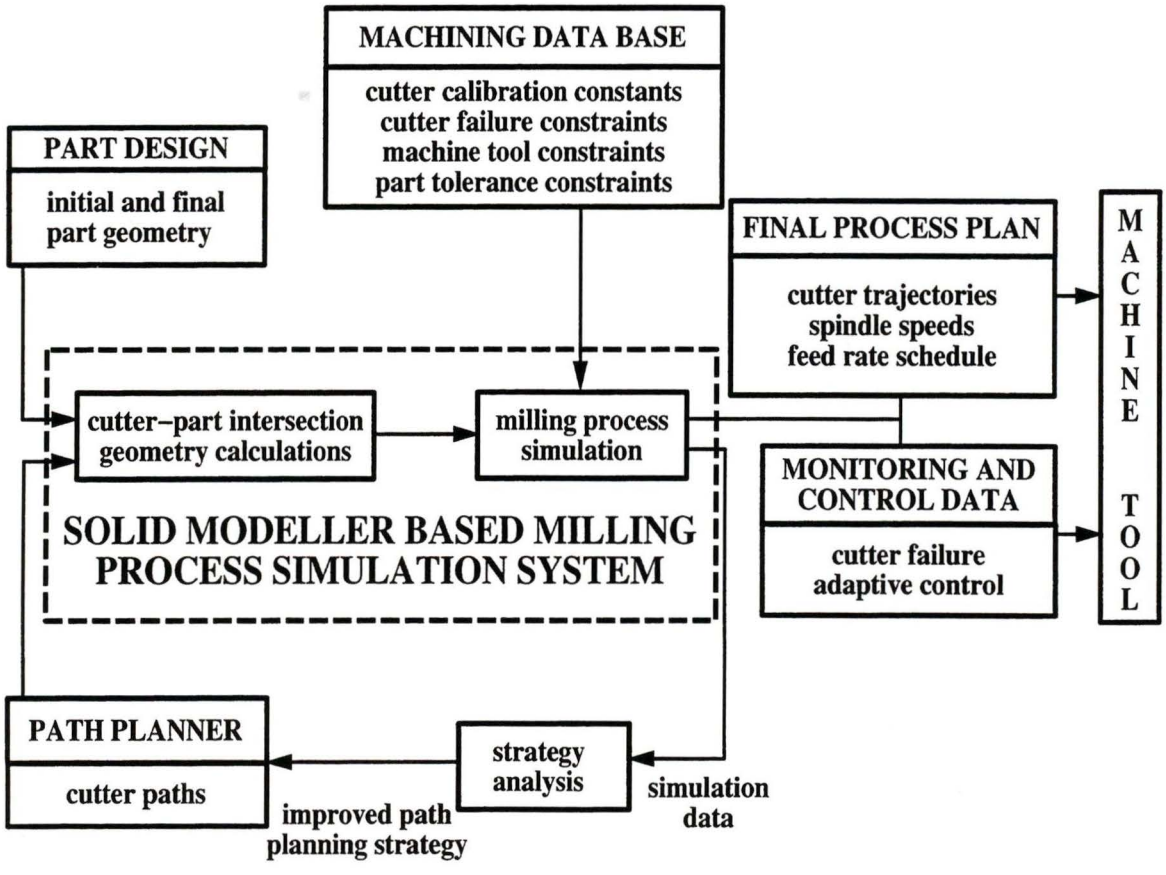

Figure 5.1: CAD assisted milling process simulator and planner.

5.1.1 The Solid Modeler

The function of the solid modeler is to generate a representation of the part and to determine the immersion geometry. The task is carried out by applying Boolean operators to a set of solid primitives, including boxes, cylinders, cones, spheres. The part is stored in a tree format, with the solid primitives being the leaves and the Boolean operations representing the nodes. This representation scheme was considered to be advantageous since during the simulation of the milling process repeated evaluation of the boundaries can be deferred.

In the case of a straight line cutter path, the immersion intervals are determined for each solid primitive as it is encountered. The immersion intervals are then classified as either in cut or out of cut. Finally a merging of the intervals is carried out using the part geometry description tree. A list is created containing the immersion interval set for each cutter path location. The procedure is capable of recognizing those immersion intervals that remain unchanged from one cutter location to another and will skip them. A further step is required for helical cutters to completely determine the length of the flutes in cut. The part surface is flattened and the intersection of each flute with the cutting zone boundaries is determined. Five intersection situations, each one with its own axial limits, have been identified.

5.1.2 Milling Process Modeling

The Material Removal Rate (MRR) milling process model is used extensively by researchers in the simulation of cutting processes. The model assumes that cutting forces are proportional to the removal rate and therefore cannot predict instantaneous forces. However, knowledge of the instantaneous cutting forces is essential in checking the shank breakage or excessive deflections. Altintas and Spence used the mechanistic

model developed by Tlusty and MacNeil to eliminate this drawback.

The mechanistic model states that for an axial element the cutting forces on each tooth j have a tangential $dF_{t,j}$ and a radial $dF_{r,j}$ component

$$dF_{t,j}(\phi, z) = K_t \cdot s_t \cdot \sin\phi(z) dz \tag{5.1}$$

$$dF_{r,j}(\phi, z) = K_r \cdot dF_{t,j}(\phi, z) \tag{5.2}$$

where $\phi(z) = \phi + j \cdot \phi_c - k_\psi \cdot z$ is the instantaneous immersion angle at axial location z. The variables appearing in the above equation are ϕ, the instantaneous immersion angle at the tip of reference flute $j = 0$, k_ψ, the helix angle constant, and, ϕ_c, the angle between two adjacent flutes. The specific cutting pressure, K_t, and the radial/tangential force ratio, K_r, are defined as

$$K_t = M_t \cdot \overline{h}^{-P_t} \tag{5.3}$$

$$K_r = M_r \cdot \overline{h}^{-P_r} \tag{5.4}$$

with M_t, M_r, P_t and P_r constants and $\overline{h}$ is the average chip thickness.

For a cutter with j teeth, the average forces are

$$\overline{F}_x = s_t \cdot K_t \cdot (R + S \cdot K_r) \tag{5.5}$$

$$\overline{F}_y = s_t \cdot K_t \cdot (-S + R \cdot K_r) \tag{5.6}$$

where parameters S and R are dependent on the cutter immersion geometry. The expressions of $\overline{F}_x$ and $\overline{F}_y$ allow the calculation of K_t and K_r. Finally, for various $\overline{h}$, the cutting constants M_t, M_r, P_t, and P_r are calibrated by measuring the correspondent average forces.

To calculate the instantaneous cutting force, $\Theta = arctan K_R$, representing the angle between the tangential and resultant force vectors, was introduced. Θ was shown to be constant at a fixed position along the cutter path. Cutting forces are

found by integrating the expressions of the instantaneous cutting forces with respect to the axial depth of cut between the two limits defined by the five contact cases. This method is more efficient than the differential element summation approach used by Takata [23].

5.1.3 Constraint Modeling and Feed Rate Scheduling

The spindle speed is selected according to the recommendations suggested by the literature. The axial depth and radial width of cut are assumed to be selected based upon part geometry and cutter diameter. Feed rates are determined by constraints, such as tooth breakage, torque and power, maximum resultant force and dimensional surface error, imposed on the cutting conditions. Under these constraints, the feed rate is calculated; and the minimum value is selected by the simulator for use in the cutting process.

This method of determining feed rate is very efficient for application at a fixed point along the cutter path. In the case of face milling operations, due to the multiple cutter immersion intervals, it is difficult to create continuous feed rate planning using this approach. The solution is to sample at small increments along the cutter path and to select the smallest feed rate. Curve fitting is then used to generate continuous feed rate planning.

5.1.4 Solid Modeler Based Process Simulation System. Advantages and Limitations

The solid modeler based process simulation system, introduced by Altintas and Spence [2], takes part and stock geometry and predicts the milling forces of the cutting process. The system produces simulation results with a good agreement with

the measured milling forces. It is for this reason that the approach is considered for implementation into our Sculptured Part Intelligent Rough Machining. An analysis of the milling process simulator provided some pointers for the future modifications.

However, the present solid modeler based simulation system has a few limitations that impede its direct use in our research. First, the simulation system is based upon Constructive Solid Geometry (CSG) representation, so the complexity of the modeled parts is limited by the possible combinations of the solid primitives. In addition, the amount of time that the system requires to compute the intersection of the cutter with each primitive is considerable. For this reason, the CSG model should be replaced with meshed surface representation, allowing for higher degree of part complexity, and dedicated intersection calculation algorithm. On the other hand, the determination of the instantaneous and average forces necessitates extensive calculations. Since these forces are not needed in the IRM approach, the calculations involved are eliminated. Finally, in order to calculate the values of the cutting coefficients, K_t and K_r, four constants, M_t, M_r, P_t and P_r, are determined through cutting tests. No explicit correlation between these constants and the cutting data is produced during these tests. So every time a new type of cutter, part material, and cutting condition is introduced, a new set of tests has to be carried out. This problem can likely be solved by conducting a systematic examination of the model for different cutting conditions and by incorporating the results into a comprehensive database.

5.2 A Modified Machining Process Model for the Sculptured Part Intelligent Rough Machining

In most cases much more attention has been attributed to the average and/or instantaneous cutting force rather than to its maximum value. Nevertheless, the maximum

cutting force is considered as the main factor in tool breakage and excessive deflection, so an in-depth study is needed.

5.2.1 Objectives

An algorithm for the feed rate scheduling has been previously discussed. An analysis of the procedure revealed that considerable improvements are needed in some areas. The objectives of this research include:

- to create a general database of cutting force coefficients, K_t and K_r. Cutting tests are to be carried out for a variety of cutting conditions. K_t and K_r values, under different cutting conditions are to be calculated from the cutting force equations.
- to offer a better solution for the feed rate scheduling problem. The specifics of the IRM require that time spent for the calculation of the immersion intervals and determination of the cutting force to be minimal.
- to increase the accuracy of the milling process simulator. Presently, reported values for the predictions vary from -15.8 to 28.9 percent.
- to implement the adapted machine process model into the IRM.

5.2.2 The Concept

Variation trends for the specific cutting pressure K_t, tangential/radial force ratio K_r and cutting force F can be extracted from force measurements. By using Equations (5.7) and (5.8), it was possible to calculate K_t and K_r from cutting data obtained

from parameter varying cutting tests.

$$K_t = \frac{F_t}{d \cdot s_t \cdot \sin(\phi)} \tag{5.7}$$

$$K_r = F_r/F_t \tag{5.8}$$

where, F_t is the tangential component of the cutting force (measured), F_r represents the radial component of the cutting force (measured), K_t and K_r are the cutting force coefficients (calculated), d is the axial depth of cut (varied according to the test plan), s_t is the feed rate (varied but not simultaneously with d), and ϕ is the immersion angle. Plots showing the behaviour of the two cutting force coefficients are given in Figure 5.2. K_t and K_r have a flat response with the variation of the immersion angle, ϕ, in the range 45 to 135 degrees. These results are corroborated by Gygax [12]. The average value of the cutting coefficients has been defined over this flat response interval. In this work, K_t, K_r, F_t, and F_r represent the averaged values.

To determine the behaviour of K_t, K_r, F_t, and F_r, the feed rate, s_t, was increased from 0.19 mm/rev/tooth to 0.64 mm/rev/tooth. Figures 5.3 and 5.4 are illustrations of the change of cutting coefficients with the variation of feed rate from the minimum to the maximum value. The analysis of cutting tests showed that the magnitude of the specific cutting pressure is inversely proportional to the feed rate. Tests conducted with different end mills have led to the same conclusion. In Figure 5.4, the tangential/radial force ratio shows a decrease with the increase in feed rate.

Variation of K_t and K_r with the axial depth of cut, from cutting tests conducted with a new tool, are illustrated in Figures 5.5 and 5.6. In Figures 5.7 through 5.10 cutting parameters, such as cutting speed and entry angle, show little influence over the magnitudes of the cutting force coefficients. Appendix C contains more plots similar to those presented above.

Other parameters, like cutter wear and geometry and workpiece material, might

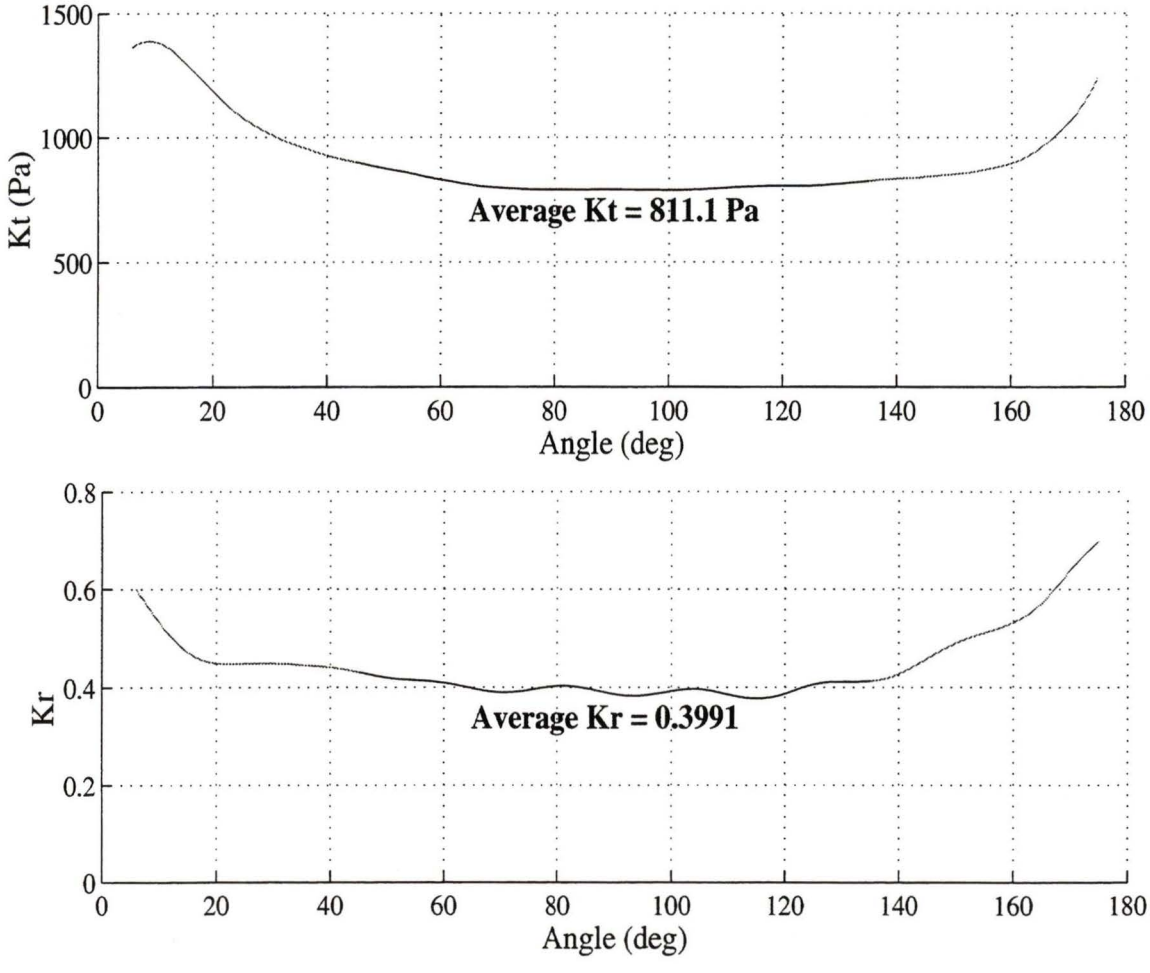

Figure 5.2: K_t and K_r as a function of the immersion angle.

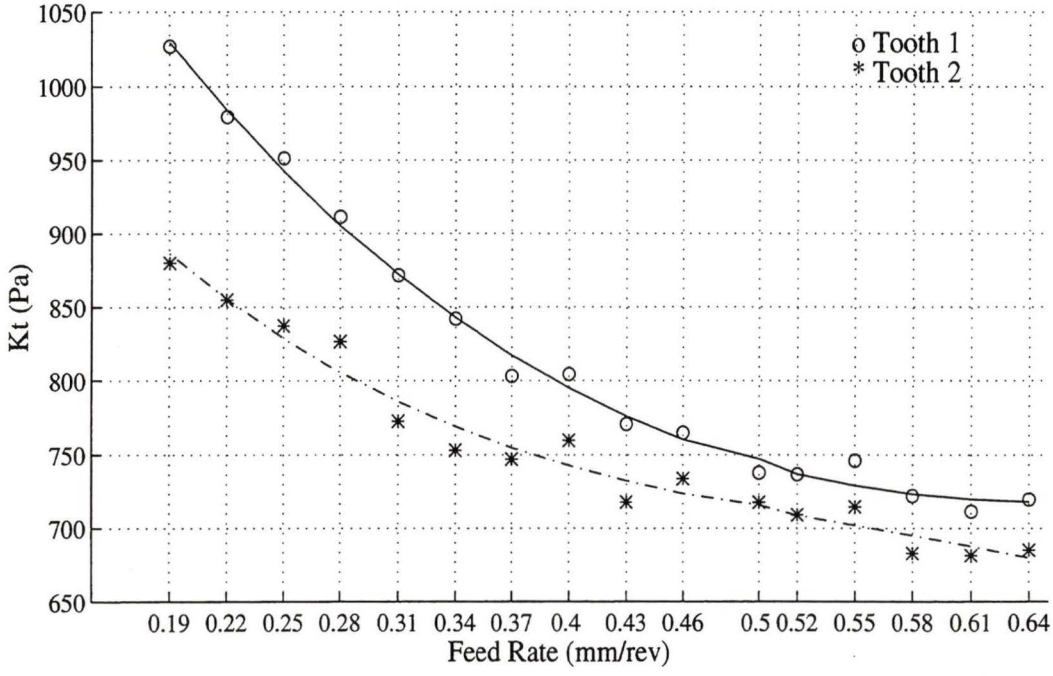

Figure 5.3: Average K_t as a function of the feed rate.

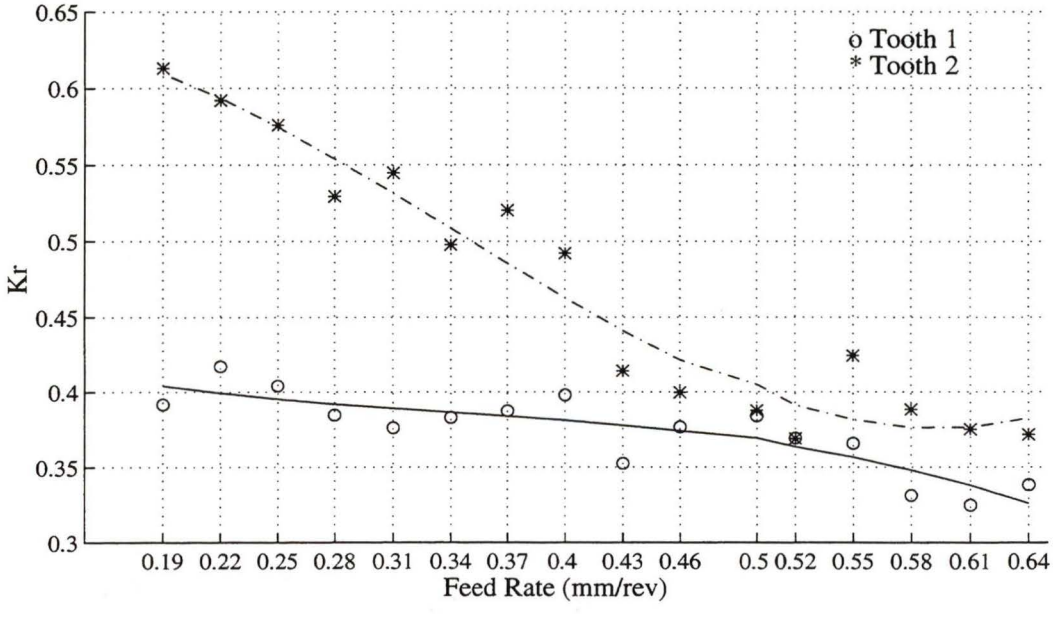

Figure 5.4: Average K_r as a function of the feed rate.

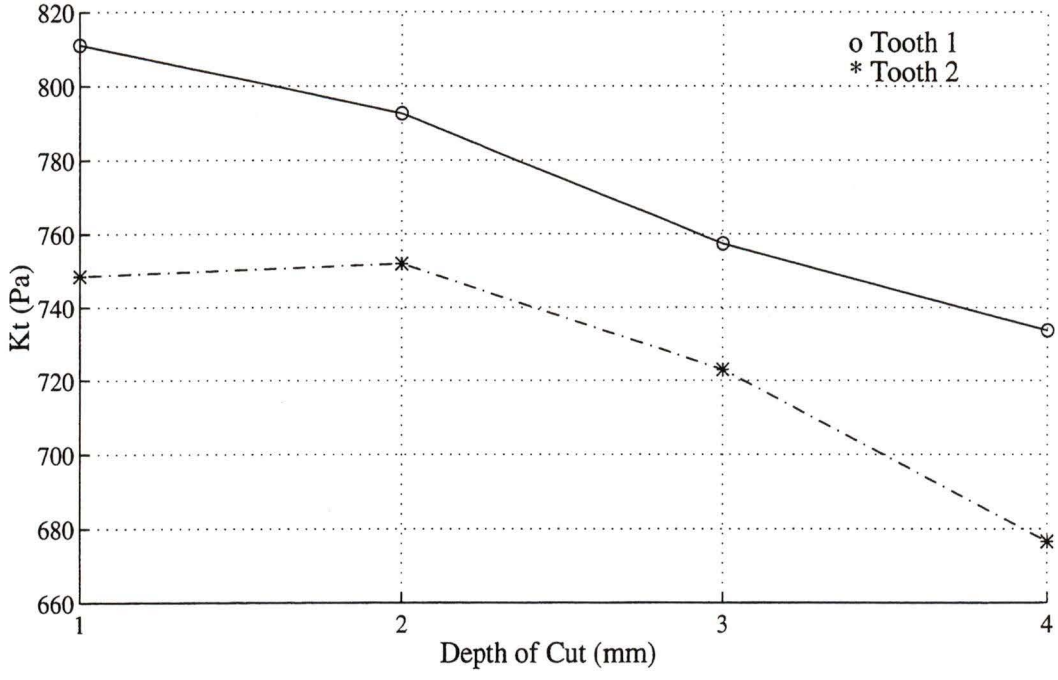

Figure 5.5: Average K_t as a function of the axial depth of cut.

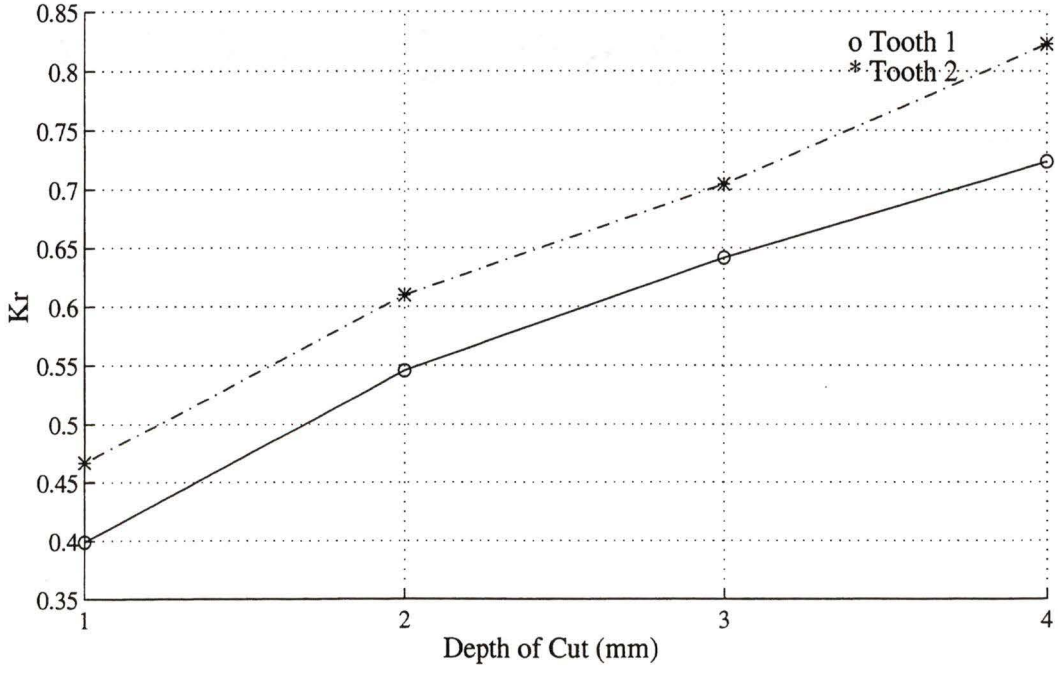

Figure 5.6: Average K_r as a function of the axial depth of cut.

also affect the cutting force coefficients. A milling cutter, which had a pronounced tool wear, produced different results than those obtained with the new tool.

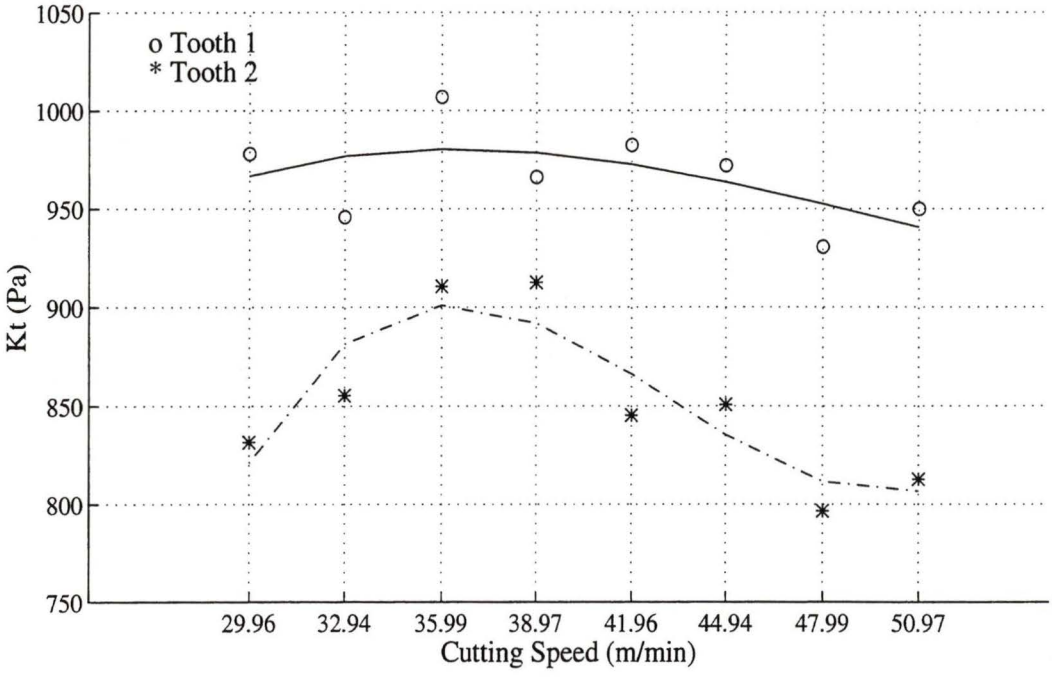

Figure 5.7: Average K_t as a function of the cutting speed.

To study the compounded effects of the cutting parameters, a 3D representation of K_t and K_r as a function of feed rate and axial depth of cut was produced. A procedure that generates the meshed surface starting from two variation plots was devised. First, two curves are selected from the array of plots that correlate K_t and K_r to cutting data (i.e. feed rate, axial depth of cut, etc.). Next, the intersection point of these curves is determined; and a meshed surface is obtained by generating similar curves over the range of parameter variation. The resulting mesh is coarse and jagged, making it difficult to find a mathematical representation, so a polynomial curve fitting is applied to the original curves. Finally, the whole generation process is repeated.

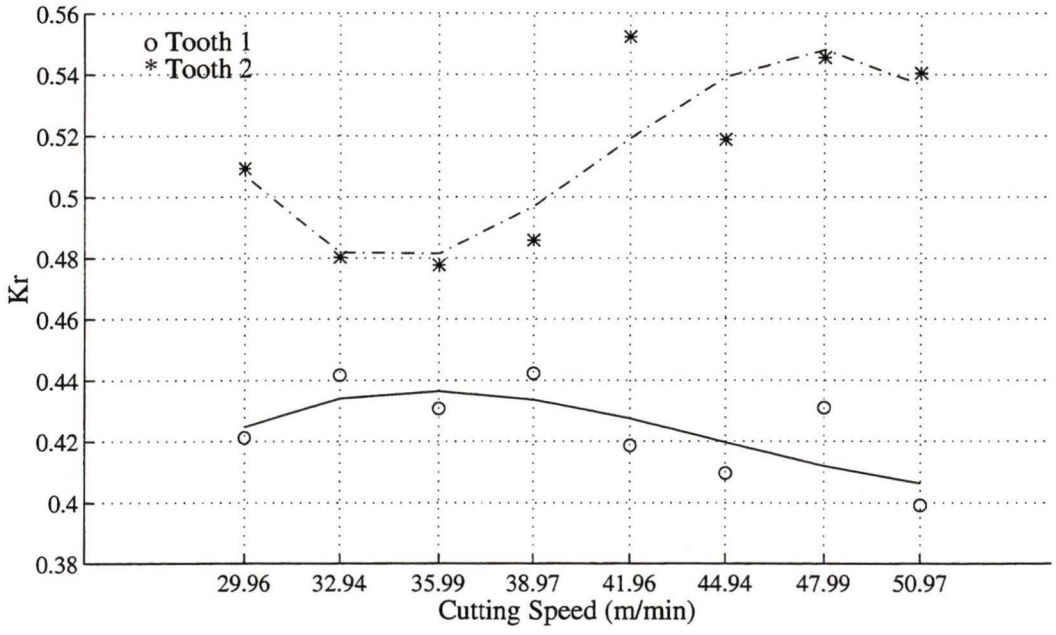

Figure 5.8: Average K_r as a function of the cutting speed.

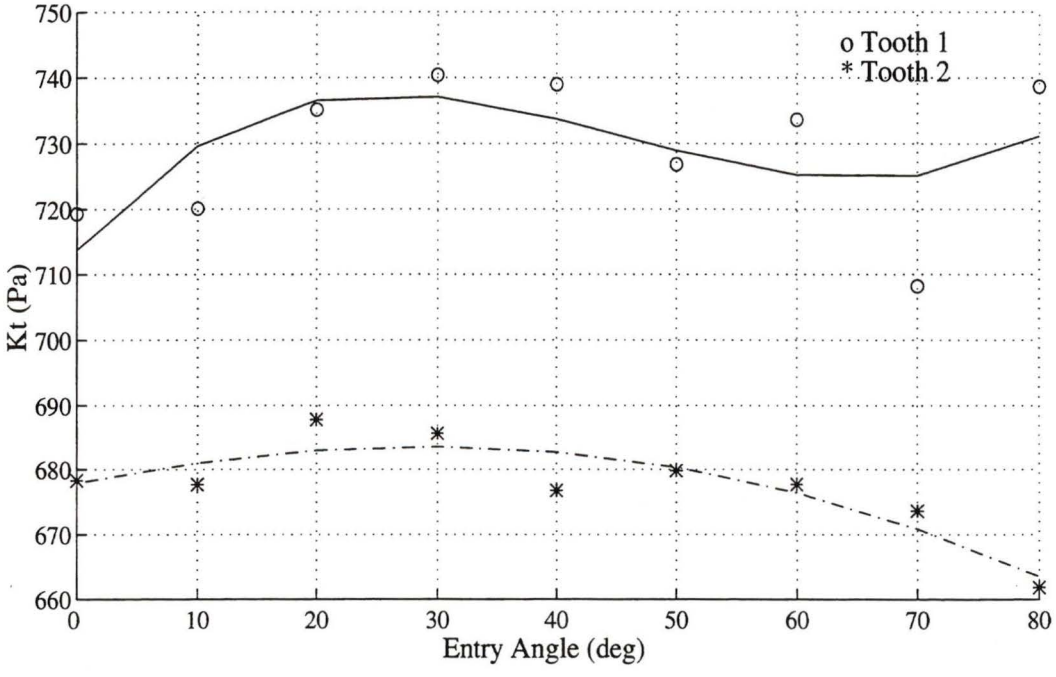

Figure 5.9: Average K_t as a function of the entry angle.

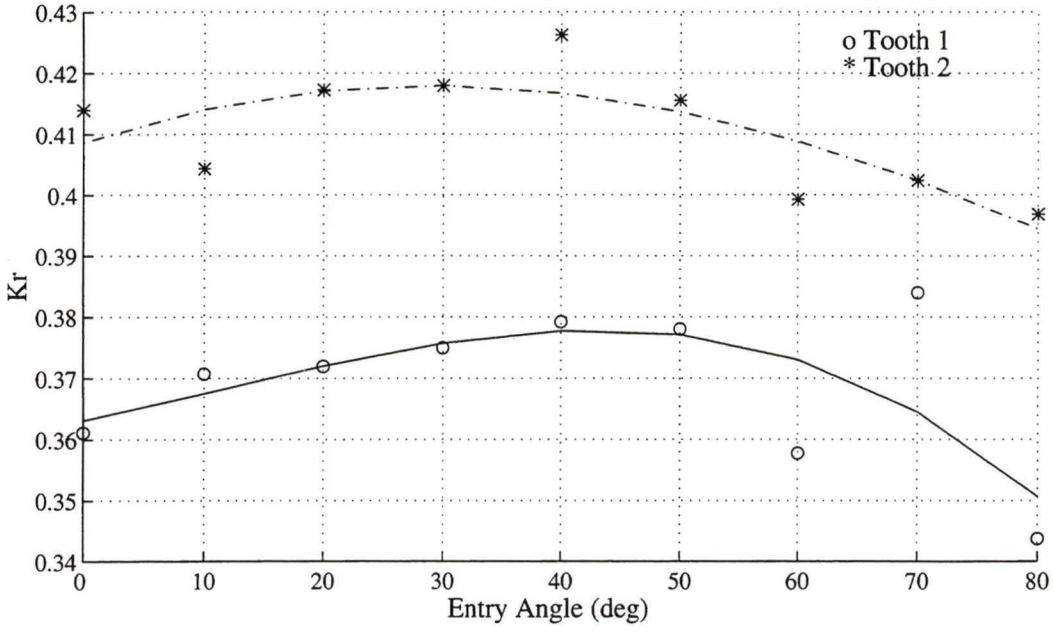

Figure 5.10: Average K_r as a function of the entry angle.

In the example that follows, a meshed surface is generated from two curves, illustrated in Figure 5.3 and 5.5, relating the variation of K_t to the feed rate and axial depth of cut. Determination of the intersection point is based on the fact that the curves were originally developed through cutting tests. All machining parameters for these tests were constant but one. By using B-spline interpolation [20], specific cutting pressures were calculated for the common feed rate and axial depth of cut. Because of experimental errors, the two values were different but within 5 percent. Consequently, the curves were shifted towards the median value of K_ts. In order to produce the meshed surface, the assumption that the variation of K_t follows the slope of the initial curves throughout the cutting parameters' range is made. Practically, the development of the surface consisted of adding parallel curves, identical to the initial ones, which extended over the whole data range. Figure 5.11 illustrates the resulting curves and their spacing, which correspond to the discrete values of the

cutting parameters. To improve the prediction accuracy a smoothing of the surface

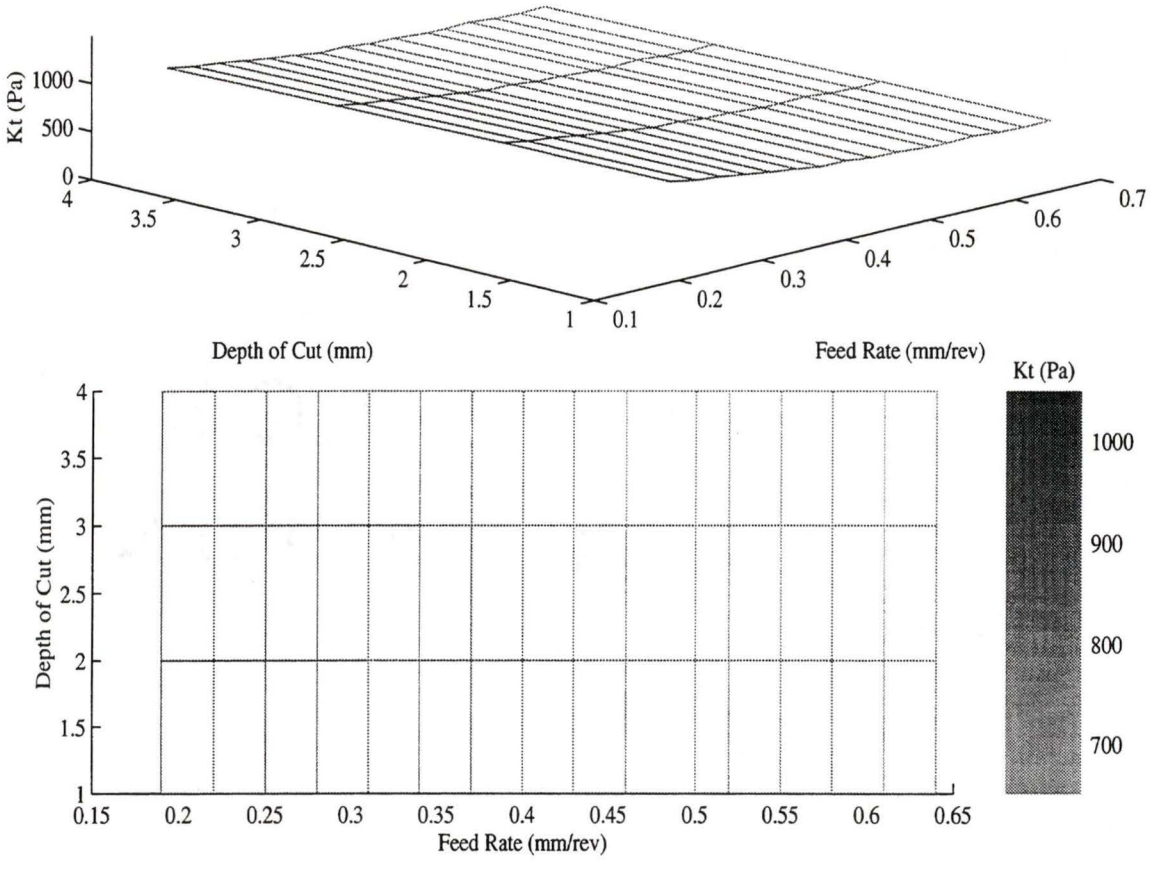

Figure 5.11: Coarse mesh.

was performed. The density of the curves was increased 25 times and they were also represented as polynomials of order 3. The result of the refining process is shown in Figure 5.12.

When the effect of a third parameter is investigated, the meshed surface transforms into a solid representation. The generation principle is similar to the one described above. Figure 5.13 shows the behaviour of K_t subjected to the added influence of cutting speed. As observed, the increase in thickness is very small, which denotes

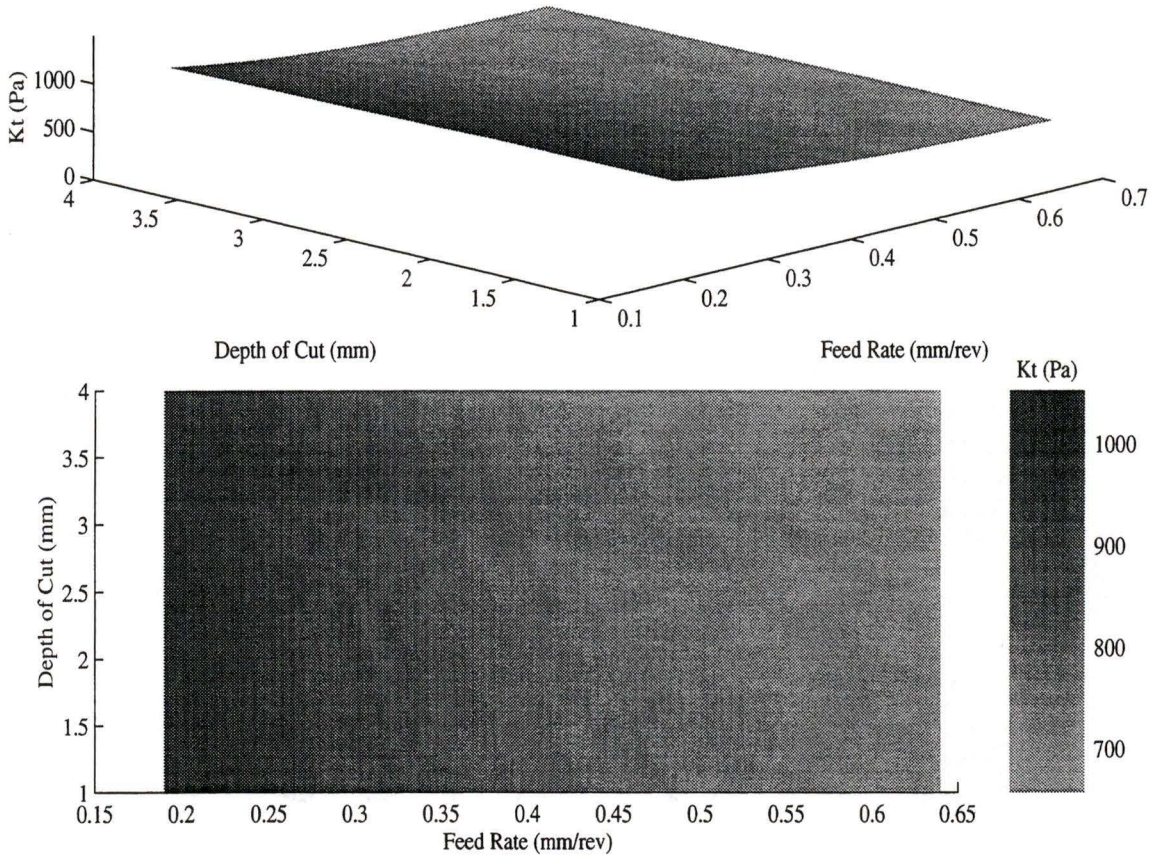

Figure 5.12: Final representation of the specific cutting pressure surface.

a comparable impact of the last introduced parameter. A similar conclusion was

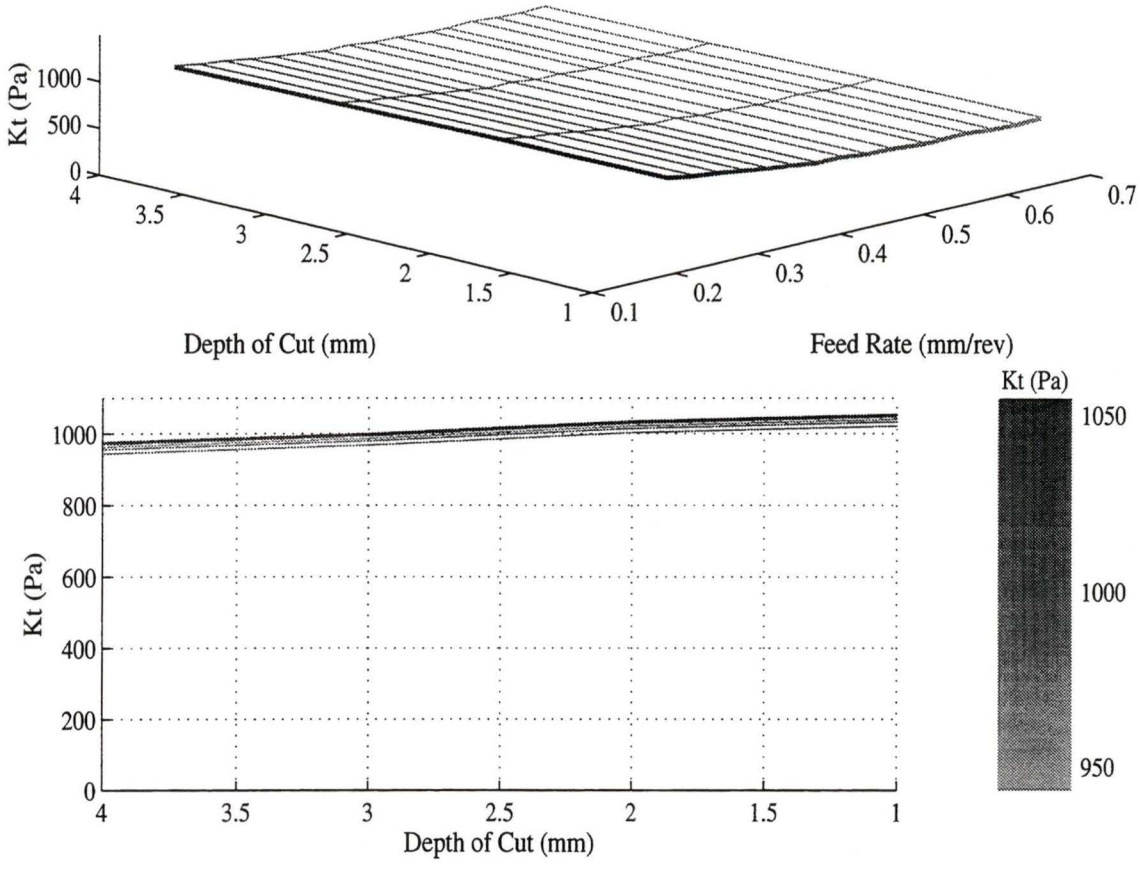

Figure 5.13: K_t as a function of feed rate, axial depth of cut, and cutting speed.

reached for the effect produced by the entry angle. That means that in order to calculate K_t and K_r, the study of the bi-parameter case is sufficient.

5.2.3 Quality of the Concept

The assessment of the machining process model consists of checking the initial requirements imposed in section 2.2. Following a point by point comparison is presented.

1. *Easy to use.* Predictions of the cutting force coefficients are obtained by interpolating for the specific cutting data. A demonstration of the procedure is included in Chapter 6.

2. *Low computational cost.* In the manufacturing phase, especially when sculptured parts (usually one of a kind) are involved, a lot of time can be spent on data preparation. In the frame of this research, a database, containing model representations for the machining cases that are to be used most frequently, is created. Accessing the knowledge base later on becomes fast and computationally insignificant.

3. *Specific design.* Specific design was considered to be an asset because it implies minimum computational cost. This means that the proposed force model is an application oriented package, which can be easily adapted to other milling operations by appropriately modifying its inputs. Factors that were considered when customizing the machine process model for use in the roughing operation of the sculptured parts include

   - representation of the sculptured part as a meshed surface.
   - application of contour mapping technique in the cutter path generation phase.
   - reduced number of metal alloys and milling cutters used by a company that produces dies or moulds.
   - boundaries of the machining parameters are selected according to cutting standards and trial testing. Limitations of the force measurements were imposed by practical reasons or the dynamometer itself.

4. *Few cutting tests required to generate the machining process model.* Due to the assumption made in the developing stage, only a few tests were necessary to

produce the initial variation curves.

5. *Accuracy of the predictions.* Available published data on the accuracy of cutting force predictions show the following spread

   - within 10 percent, for the flexible system model, and as much as 125 percent, for the rigid system model [14].
   - 5 to 20 percent [29].
   - -15.8 to 28.9 percent for the deflection model [8].

   To verify the accuracy of predictions, cutting data were chosen such that there was no overlapping with the values that generated the initial curves. Two milling cutters were used and the cutting tests carried out were identical for both tools. One of the cutters was the same cutter that produced the machining process model, while the other one was brand new but otherwise similar. Figure 5.14 illustrates the feed rates and depths of cut that were selected for the tests together with the initial values. The upper right corner was avoided due to the extreme cutting forces involved, where extreme refers to the capabilities that were built-in the dynamometer. The same cutting data were input into the machining process model, and predictions for K_t, K_r, F_t, F_r and F were obtained. Graphical representations of the differences between the test data and predicted values for the new tool are presented in Figures 5.15 through 5.17. The actual values have been assembled in two tables and are included in Appendix D.

   Two observations are noteworthy. First, the majority of differences for the worn tool indicate positive values, while for the other cutter the differences are mostly negative. And second, the maximum error recorded in the first case is larger than the error resulted in the second case. Since all test parameters were

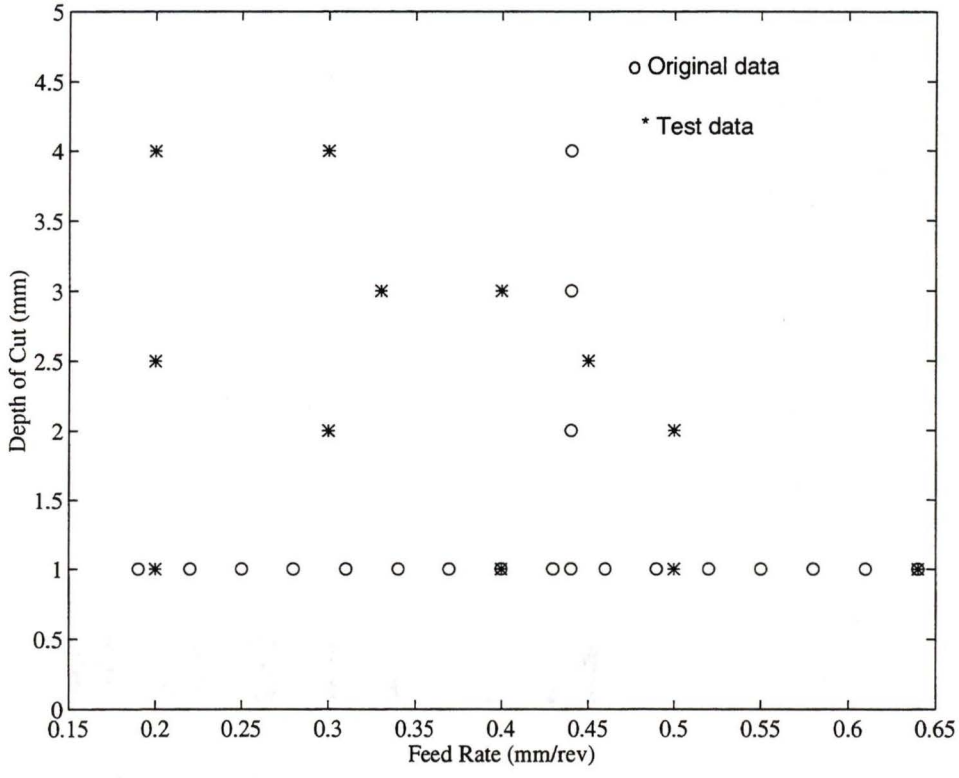

Figure 5.14: Selection of cutting parameters to be used for verification of predictive model.

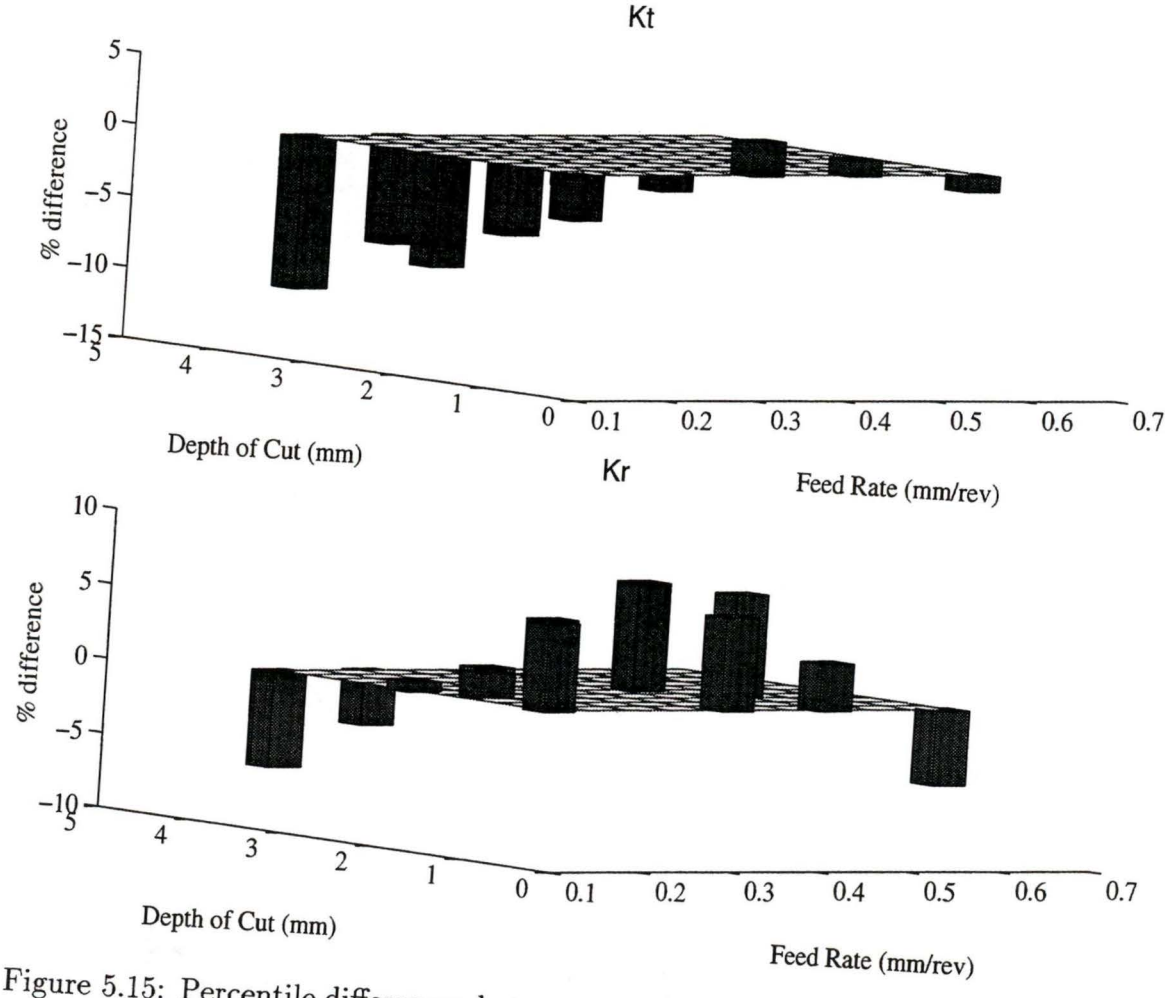

Figure 5.15: Percentile differences between test and predicted data for K_t and K_r.

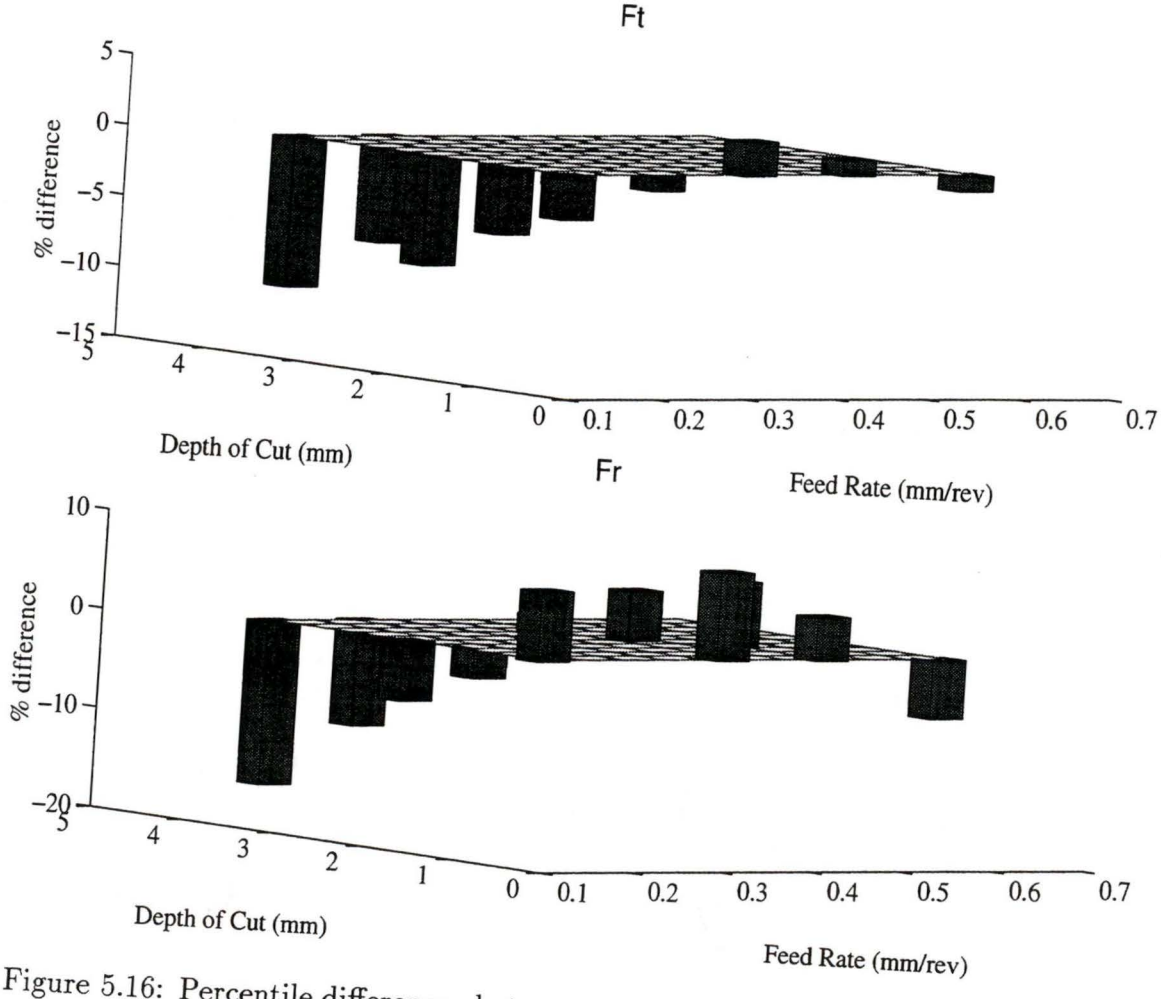

Figure 5.16: Percentile differences between test and predicted data for F_t and F_r.

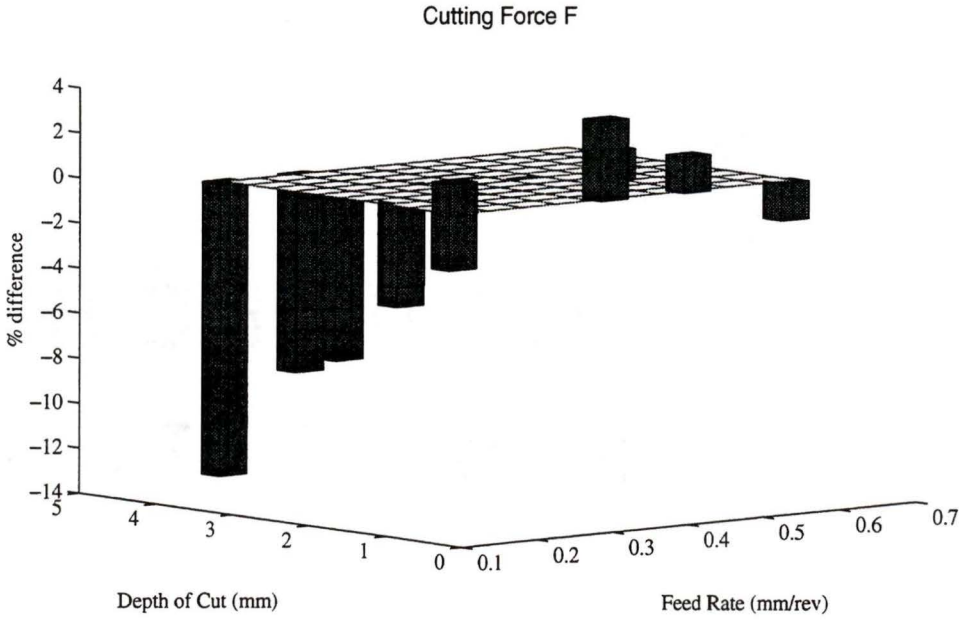

Figure 5.17: Percentile differences between test and predicted data for total cutting force F.

identical, with the exception of the tool's wear, closeup shots of the cutting edges were taken. Figure 5.18 shows an image of one of the flutes of the worn out tool. It is obvious that the cutting edge is chipped, so an increase in cutting force is normal. Pictures of the second tool revealed no elements of concern, which confirmed the initial belief regarding the effect of cutter wear.

In the end, a short statistical analysis was produced [3]. The location and spread of the differences between test and prediction values are given by the mean and standard deviation of data. Calculated results for the two groups of tests are $\bar{x}_1 = 8.3464$ percent, $x\delta_{n1} = 6.9770$ and $\bar{x}_2 = -2.7784$ percent, $x\delta_{n2} = 4.5725$. Next, data were grouped into five bins; and it was found that a normal distribution best described the data. Knowing the type of distribution, it was possible to show that 95 percent of future predictions will yield differences in the range $\bar{x} \pm 1.96 \cdot x\delta_n$. Thus, for the first group the range is 8.3464 ± 13.6749

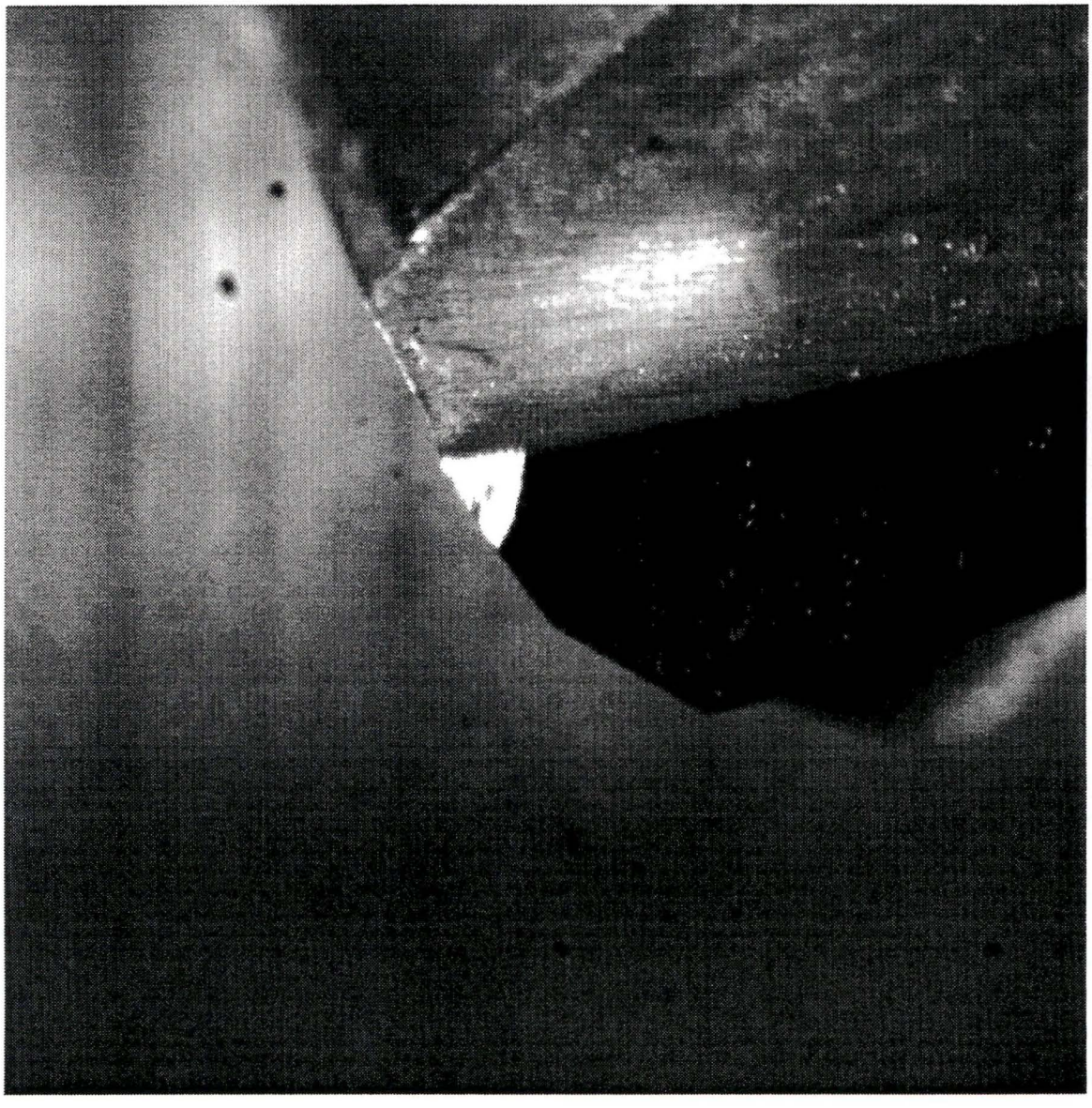

Figure 5.18: Cutting edge of the original milling cutter.

percent; and for the second group the range is -2.7784±8.9621 percent. Finally, in order to describe the future mean values, a confidence interval is quoted. The formula used is $\bar{x}\pm t \cdot x\delta_n/\sqrt{(n)}$ where t is a critical value from the t-table for a two-sided test using the appropriate degrees of freedom n. The values of the confidence intervals are 8.3464±4.2184 percent and -2.7784±2.7646 percent respectively.

In summary, the conclusions derived from the analysis of the machine proces model are:

- The adapted cutting force model proves adequate, considering the fulfillment of the initial requirements.
- Due to preference for overpredicting cutting forces, the cutting force model is conservative.
- Implementation of wear in the model could improve the accuracy of predictions.

Chapter 6

Implementation of the Machining Process Model

A modified machining process model was introduced in Chapter 5. The features of this new model were shown to satisfy the requirements imposed earlier, in Chapter 2. Even if this tool can be used as stand alone, for prediction of the cutting forces, it is the intent of the author to integrate the predictive system into the IRM approach.

The work of Vickers and Bradley [11] provided information regarding the time response of the Victor VM-5 four-axis machining center, equipped with a FANUC 6MB controller. They carried out velocity measurements in Direct Numerical Control (DNC) mode and memory mode, with three repetitive steps of linear table motion, at a constant feed rate of 2544 mm/min. In DNC mode it was observed that both the acceleration and deceleration phases require 0.02 s to complete, and 0.12 s are necessary for the processing of the next block of instructions. While these times are similar for any size linear movement, the time interval necessitated for the execution of the linear step varies with its size. In conclusion, the shorter the table's advancement, the larger the waiting time/execution time ratio becomes. Similar observations were

made in the memory mode operation. The only difference was that the dwell time was reduced from 0.12 to 0.029 s, which was explained by the controller not checking the buffer prior to executing every command. Another controller, the FANUC 10T, was also investigated by Vickers and Bradley with comparable results.

Based on these conclusions, an efficient machining strategy for sculptured parts can be devised. It was shown in Chapter 2 that the IRM approach proposed the reduction of the machining time by heuristic tool path pattern generation and machining parameter optimization. Since the study of the tool path generation is beyond the scope of this research, an improvement of the machining parameter selection is presented.

In order to check the IRM approach together with the machining process model, a test was planned. Figure 6.1 illustrates a milling situation in which a wedge-shaped workpiece is machined at a maximum cutting force of 500 N. At this point

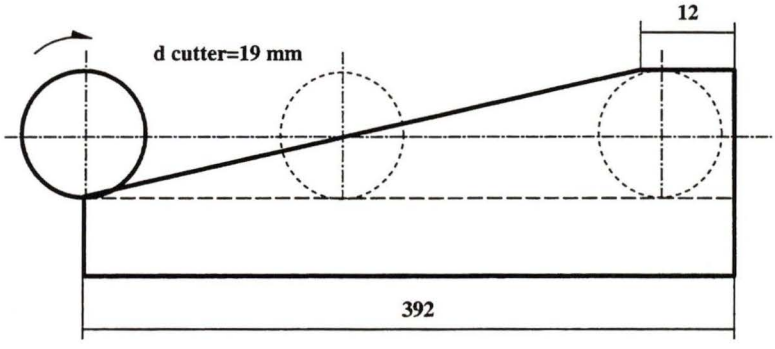

Figure 6.1: Test workpiece for machining process model.

the limiting value of the cutting force was chosen somewhat arbitrarily, reflecting chatterless cutting conditions. The machining parameter range that the proposed cutting force model supports was another reason for the above selection. A more general case would take into consideration other constraints, such as

- *maximum and minimum feed rate*, which could be determined by either im-

posing a tooth breakage condition or simply being a physical constraint of the milling machine. The tooth breakage constraint, proposed by Yellowley and Gunn [2], states that

$$s_t = \frac{h_{max}}{(sin\phi)_{max}} \tag{6.1}$$

where $(sin\phi)_{max}$ depends on the immersion angle ϕ.

- *maximum and minimum depth of cut*, is usually a constraint determined by the type and geometrical characteristics of the milling cutter.

- *maximum cutting torque and power.* Expressions for the feed rate can be derived from the definitions of torque: $T = r_c \cdot F_t$, where r_c is the cutter radius, and power: $P = T \cdot \omega$, where ω is the spindle speed.

- *maximum cutting force.* Since the tensile stress due to the bending moment is far more important than the shear stress produced by the cutting torque, in practice, the cutting force is an important constraint. Based on Equations 1.1 through 1.3 and applying the procedure presented in [2], the maximum feed rate derived from the maximum cutting force condition can be calculated.

Other supplemental conditions may be imposed to further constrain the calculation of feed rate.

As demonstrated at the beginning of the chapter, for short linear movements of the table, either a lot of time is spent waiting for the next instruction to be processed or the commanded feed cannot be attained. Ideally, to maintain a constant material removal rate throughout machining, a continuous feed rate adjustment is desired. In order to resolve these opposing tendencies, a compromise was reached. Average feed rates mostly used were in the range 250 to 500 mm/min, which is the equivalent of 4 to 8 mm/s. Obviously, when comparing this velocity to the one at which Vickers

and Bradley carried out their experiments, the acceleration/deceleration times are insignificant. Assuming a 1 mm step for the advancement of the cutter, a fair simulation resolution for the feed rate is obtained, and in the same time the commanded movements of the table are not too short. To eliminate the last inconvenience, the idle time between two successive instructions, a clustering of the table motion intervals is applied. The clustering is determined such that the predicted cutting force is in the range *imposed cutting force+10 percent.* Consequently, a reducing of the number of instructions is achieved, resulting in less time wasted for their processing.

Calculations of the total machining time were carried out for the part in Figure 6.1 with constrained maximum cutting force from 500 to 800 N and depth of cut of 2 mm. The planning of the feed rate is shown in Figure 6.2 for both cases, clustered and non-clustered. Figure 6.3 illustrates the behaviour of the cutting force F in the clustered feed rate case. Initially, the advancement of the cutter was 1 mm but for the imposed load of 500 N other increments were considered as well. Figure 6.4 illustrates the results of those calculations for various maximum cutting forces. An investigation of the effect of increment size was carried out and the results are presented in Figure 6.5. The machining time savings are determined by comparing the time required to machine the workpiece with the minimum feed rate (non-clustered case), to the time needed when the clustered feed rates are applied.

Analyzing the data in Figures 6.4 and 6.5 no clear conclusion can be drawn, as what time savings one could expect for a certain maximum cutting force and/or step size. I am inclined to say that machining time savings are probably dependent on the cutter path and further experimentation is required for a general solution.

The knowledge accumulated during this exercise can be easily transferred to the IRM approach so that feed rate planning is accomplished.

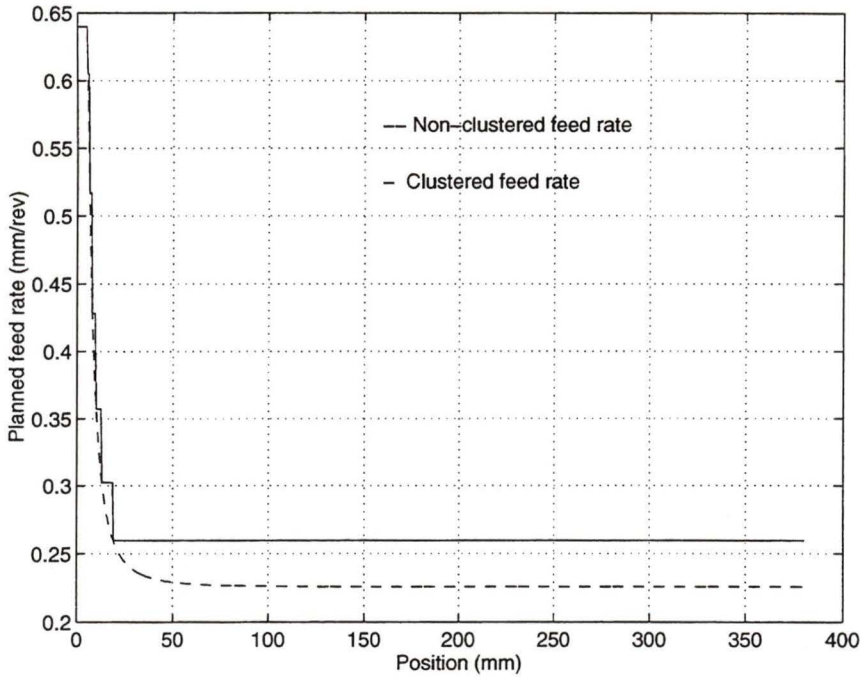

Figure 6.2: Feed rate planning for the wedge shaped part.

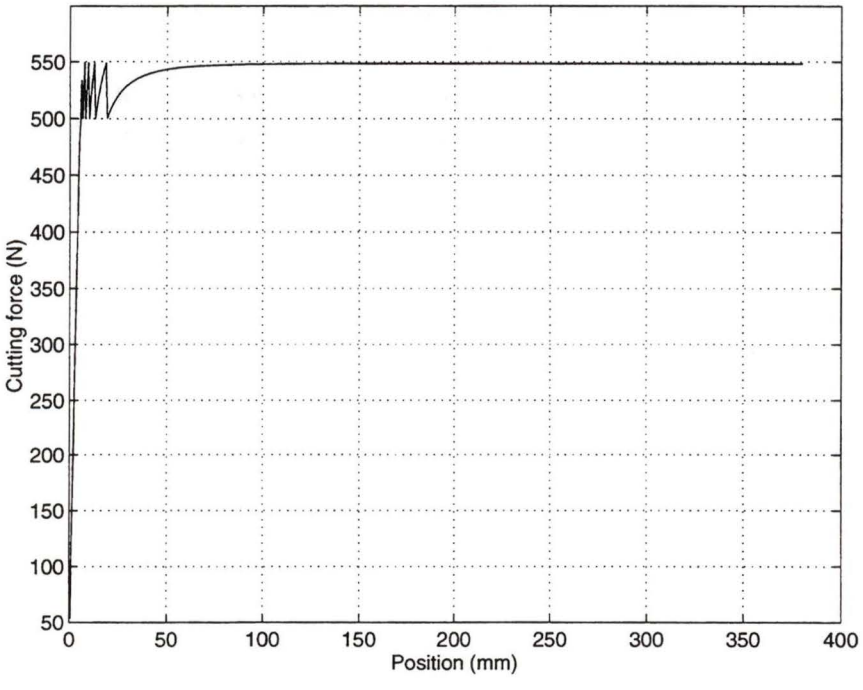

Figure 6.3: Cutting force, F, for the wedge shaped part and clustered feed rates.

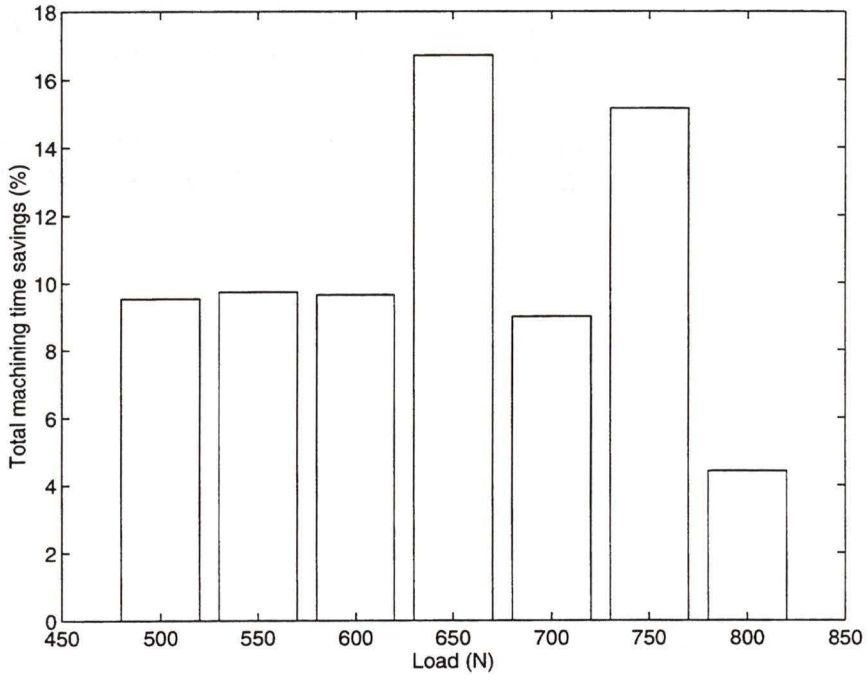

Figure 6.4: Total machining time versus constrained cutting force.

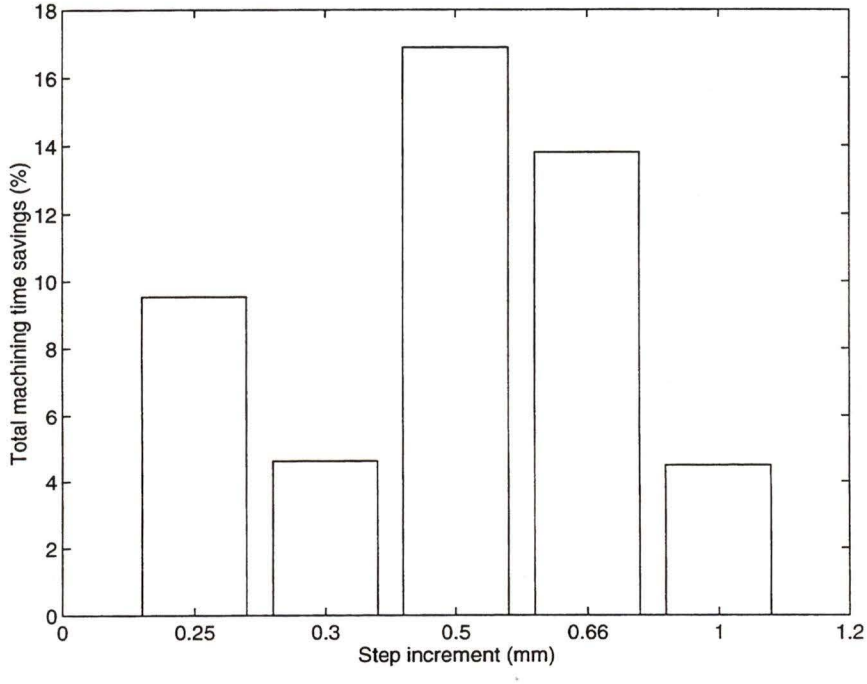

Figure 6.5: Total machining time versus calculation increment.

Chapter 7

Conclusions and Future Improvements

An overview of the research done in the area of machining process modeling was presented in the introductory chapter. An approach, the IRM, developed at the University of Victoria was introduced. In order to increase the performance of the IRM, a cutting force model was required. Opposed to the common tendency of using MRR models, a simulator based on experimental cutting data was preferred. Force measurements were carried out using a rotative dynamometer, built at UVic. Relying on the results of data acquisition during the statisticaly scheduled cutting tests, a simple and easy to implement cutting force model was proposed. The described model was tested for cutting parameters in the initial boundaries and, the predicted cutting forces were verified through machining. A good agreement between predictions and force measurements was obtained. Previously, in Chapter 6, the predictive force model was transformed such that feed rates could be planned according to the cutter path and physical and geometrical constraints. The use of the predictive model demonstrated savings of 4 to 16 percent in machining time, which translated into

increased productivity and better loading of the machine tool.

The IRM approach together with the proposed cutting force model demonstrated that the rough machining of sculptured parts can be optimized successfully. The combined effects account for as much as 55 percent less machining time compared to the case when cutting parameters were selected from machining data handbooks.

A better understanding of the cutting force modeling process was acquired during the experimental and data processing stages. Future improvements would target those areas that provide an increase in the prediction accuracy and/or a generalization of the cutting force model. Such areas of interest could be:

1. *re-design of dynamometer.* For expanding the range of cutting force measurements an increase in the rigidity of the unit is desired. For example a rotary tool holder adapter could be retro-fitted with adequate instrumentation. A more sensible full Wheatstone bridge could be used instead of the half bridge arrangement. In order to avoid the strain gauges' installation misalignment facets, which provide a flat reference surface, could be machined. Another qualitative upgrading could be the use of wireless data transmission instead of the troublesome slip rings. Improvement of the triggering device would lead to a more rigorous alignment of a multi-flutted cutter with the zero point, so cutting tests with those tools could be carried out.

2. *extension of the cutting test plan* to include different cutter geometries and milling operations and investigate other factors that were found to influence K_t and K_r (such as tool wear).

3. *improvement of the feed rate planning procedure.* Instead of calculating the total machining time for various step sizes an optimization function could be determined.

Bibliography

[1] Y. Altintas and A. Spence. End Milling Force Algorithms For CAD Systems. *Annals of the CIRP*, 40/1:31–34, 1991.

[2] Y. Altintas and A.D. Spence. A Solid Modeler Based Milling Process Simulation and Planning System. *Quality Assurance Through Integration of Manufacturing Processes and Systems*, PED-56:65–79, ASME 1992.

[3] R. Caulcutt. *Statistics in Research and Development*, chapter 2–4. Chapman and Hall, 1983.

[4] Z. Dong, H. Li, and G. W. Vickers. Optimal Rough Machining of Sculptured Parts on a CNC Milling Machine. *Transactions of the ASME*, 115:424–431, November 1993.

[5] Z. Dong, H. Li, and G. W. Vickers. *Intelligent Rough Machining of Sculptured Parts - Planning and Programming*, chapter 9. Prentice Hall Inc., 1994.

[6] Z. Dong, H. Li, and G. W. Vickers. A Fast Offsetting Algorithm for Generating 2D Tool Paths. In *Proceedings of the CANCAM Conference*, pages 680–681, Victoria, 1995.

[7] Y. Altintas E. Budak. Prediction of the Milling Force Coefficients From Orthogonal Cutting Data. *Transactions of the ASME.*

[8] N.P. Deshpande E.J.A. Armarego. Computerized End Milling Force Predictions with Cutting Models Allowing for Eccentricity and Cutter Deflections. 1991.

[9] A. Bayoumi G. Yucesan, Q. Xie. Determination of Process Parameters Through A Mechanistic Force Model of Milling Operations. *Int. J. Mach. Tools Manufact.*, 33/4:627–641, 1993.

[10] Y. Altintas G. Yucesan. Improved Modeling of Cutting Force Coefficients in Peripheral Milling. *Int. J. Mach. Tools Manufact.*, 34/4:473–487, 1994.

[11] C. Bradley G.W. Vickers. curved Surface Machining Through Circular Arc Interpolation. *Computers in industry*, 19:329–337, 1992.

[12] P.E. Gygax. Experimental Full Cutt Milling Dynamics. *Annals of the CIRP*, 29:61, 1980.

[13] S. Haykin. *Modern Filters*, chapter 6. MacMillan Publishing Co., 1989.

[14] R.E. DeVor J.W. Sutherland. An Improved Method for Cutting Force and Surface Error Prediction in Flexible End Milling Systems. *Journal of Engineering for Industry*, 108:269–279, 1986.

[15] *LabVIEW, User Manual*, 1991.

[16] H. Li. *Intelligent Rough Machining.* PhD thesis, University of Victoria, 1995.

[17] J.N. Little and L. Shure. *Signal Processing Toolbox for use with MATLAB.* The MathWorks Inc., 1988.

[18] Machining Data Handbook, 1980.

[19] M.E. Martellotti. An Analysis of the Milling Process. *Transactions of the ASME*, 63:667, 1941.

[20] *MATLAB, Reference Guide*, 1993.

[21] T. Moriwaki and E. Shamoto. Modeling and Parameter Identification of End Milling for Estimation of Dynamic Cutting Force. In *Proceedings of Pacific Conference on Manufacturing*, pages 97–103, 1994.

[22] OMEGA Complete Pressure, Strain and Force Measurement Handbook and Encyclopedia, 1995.

[23] T. Sata S. Takata, M.D. Tsai. A Cutting Simulation System for Machinability Evaluation Using A Workpiece Model. *CIRP Annals*, 38:417–420, 1989.

[24] A.J.P. Sabberwal. Chip Section and Cutting Force During the Milling Operation. *Annals of the CIRP*, 10:62, 1961.

[25] Cutting Tool Handbook, 1985.

[26] J. Tlusty and P. MacNeil. Dynamics of Cutting Forces in End Milling. *Annals of the CIRP*, 24:21, 1975.

[27] Milling Systems, 1990.

[28] R.E. DeVor W.A. Kline. The Effect of Runout on Cutting Geometry and Forces in End Milling. *Int. J. Mach. Tool Des. Res.*, 23:123–140, 1983.

[29] R.E. DeVor W.A. Kline and J.R. Lindberg. The Prediction of Cutting Forces in End Milling with Application to Cornering Cuts. *Int. J. Mach. Tool Des. Res.*, 22/1:7–22, 1982.

Appendix A

VI's Front Panel

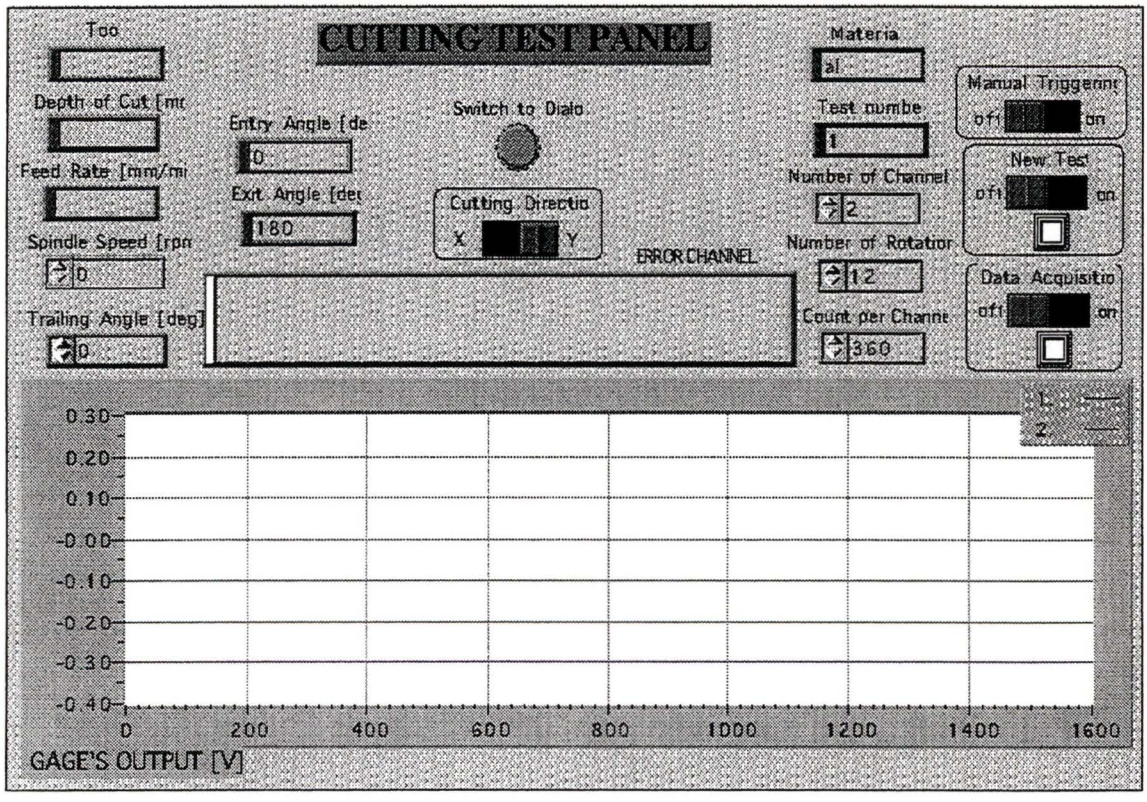

Figure A.1: The cutting test front panel.

Appendix B

Plan of Testing

Cutting Tests

March 10 - 31, 1995.

The Milling Cutters (MC) used for testing are:

1. Quinco 3/4" High Speed Steel (HSS) 2 flutes - shank diameter 1/2", length of cut 1-5/16", OverAll Length (OAL) 3-5/16";
2. HSS 3/4" 4 flutes - unknown brand and tool geometry;
3. Niagra 1/2" HSS 2 flutes - shank diameter 1/2", length of cut 1", OAL 3", uncoated;
4. Niagra 3/4" HSS 2 flutes - shank diameter 3/4", length of cut 1-5/16", OAL 3-9/16", uncoated;
5. Niagra 3/4" HSS 2 flutes - shank diameter 3/4", length of cut 1-5/16", OAL 3-9/16", coated (TiN);

6. Valenite Centre-Dex - 1 carbide insert (VC-2), diameter .980", shank .750", length of cut 1.250", OAL 3.310", rake angle , lead angle ;

7. Valenite Centre-Dex - 2 carbide inserts (VC-2), diameter 1.000", shank .750", length of cut 1.250", OAL 3.310", rake angle , lead angle ;

The cutting parameters and their variation range were:

Depth of Cut

MC1: 1.0, 1.3, 1.6, 1.9, 2.2, 2.5, 2.8, 3.1, 3.4, 3.7, 4.0 mm;

MC2: 2 mm;

MC3: .5, 1.0 mm;

MC4: 1.0 mm;

MC5: 1.0, 2.0, 3.0, 4.0, 5.0, 6.0, 7.0 mm;

MC6: .5 mm;

MC7: .5, .75 mm.

Cutting Speed

MC1: 30, 33, 36, 39, 42, 45, 48, 51, 54, 57, 60 m/min;

MC2: 45 m/min;

MC3: 45 m/min;

MC4: 30, 33, 36, 39, 42, 45, 48, 51, 54, 57, 60 m/min;

MC5: 30, 33, 36, 39, 42, 45, 48, 51, 54, 57, 60 m/min;

MC6: 117, 133, 148, 164, 180, 195, 211, 226, 242 m/min;

MC7: 148 m/min.

Entry/Exit Angle

MC1: starting angle: 0, 60; exit angle: 120, 160, 180;

MC2: starting angle: 0, 60; exit angle: 180;

MC3: starting angle: 60; exit angle: 180;

MC4: starting angle: 60, 84; exit angle: 180;

MC5: starting angle: 0, 10, 20, 30, 40, 50, 60, 70, 80, 84, 90; exit angle: 180;

MC6: starting angle: 0; exit angle: 180;

MC7: starting angle: 0; exit angle: 180.

Feed Rate

MC1: .1, .13, .16, .19, .22, .25, .28, .31, .34, .37, .4, .56 mm/rev;

MC2: .05, .065, .08, .1, .13 mm/rev;

MC3: .1, .13, .16, .19, .22, .25, .28, .31, .34, .37, .4 mm/rev;

MC4: .1, .13, .16, .19, .22, .25, .28, .31, .34, .37, .4 mm/rev;

MC5: .1, .13, .16, .19, .2, .23, .25, .26, .29, .3, .32, .35, .38, .4, .41, .43, .44, .45, .46, .47, .49, .5, .52, .53, .55, .56, .58, .59, .6, .62, .65 mm/rev;

MC6: .1, .12, .14, .16, .18, .2, .22, .24, .26, .28, .3 mm/rev;

MC7: .24, .26, .28, .3 mm/rev.

Appendix C

Plots Showing the Variation of the Cutting Force Coefficients

Variations in the specific cutting pressures, K_t, and tangential/radial force ratios, K_r,. were illustrated in Chapter 5 for a brand new tool. Figures C.1 through C.6 show the dependency of the two cutting coefficients, K_t and K_r, for a worn milling cutter.

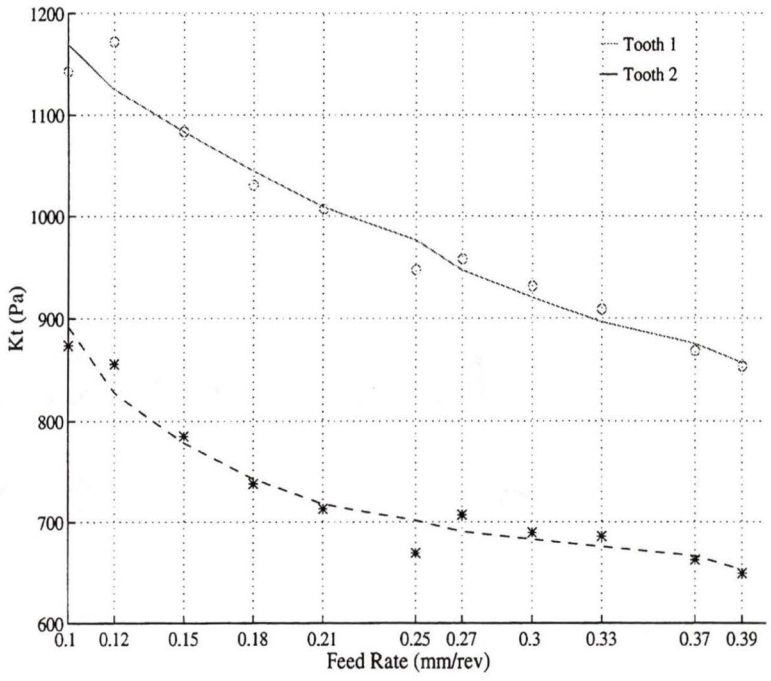

Figure C.1: Average K_t as a function of the feed rate.

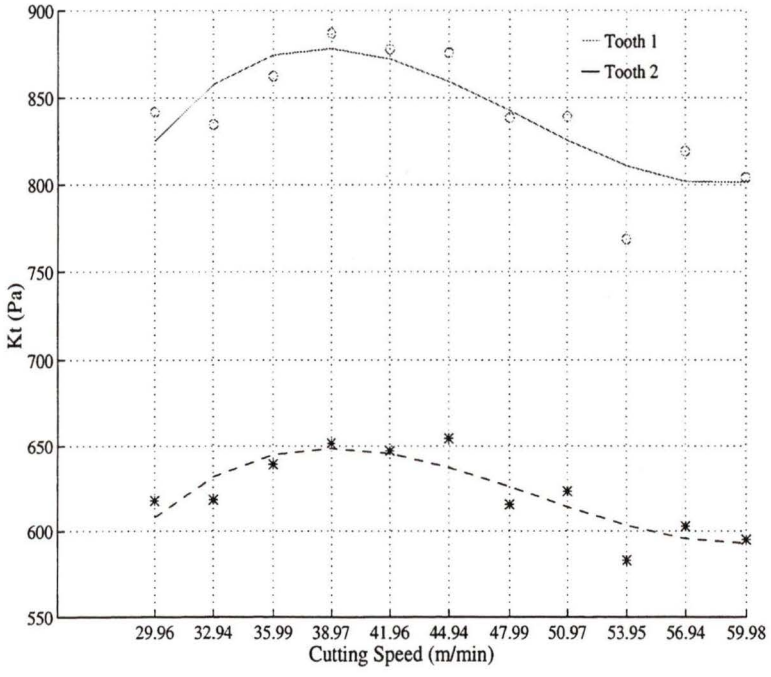

Figure C.2: Average K_t as a function of the cutting speed.

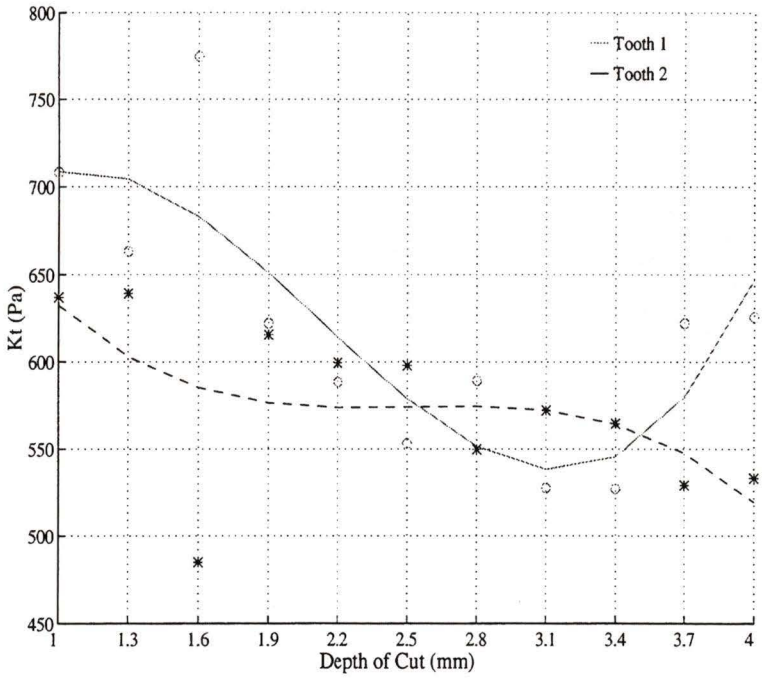

Figure C.3: Average K_t as a function of the axial depth of cut.

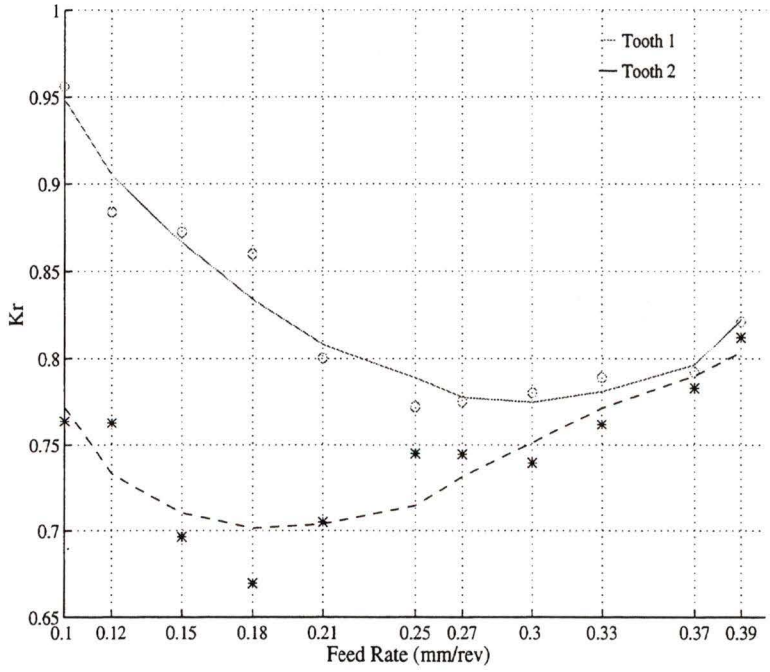

Figure C.4: Average K_r as a function of the feed rate.

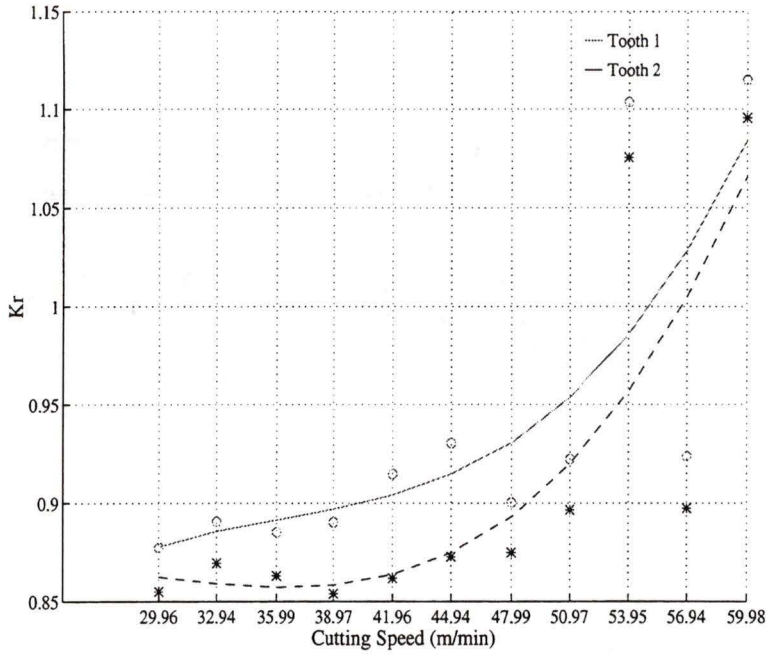

Figure C.5: Average K_r as a function of the cutting speed.

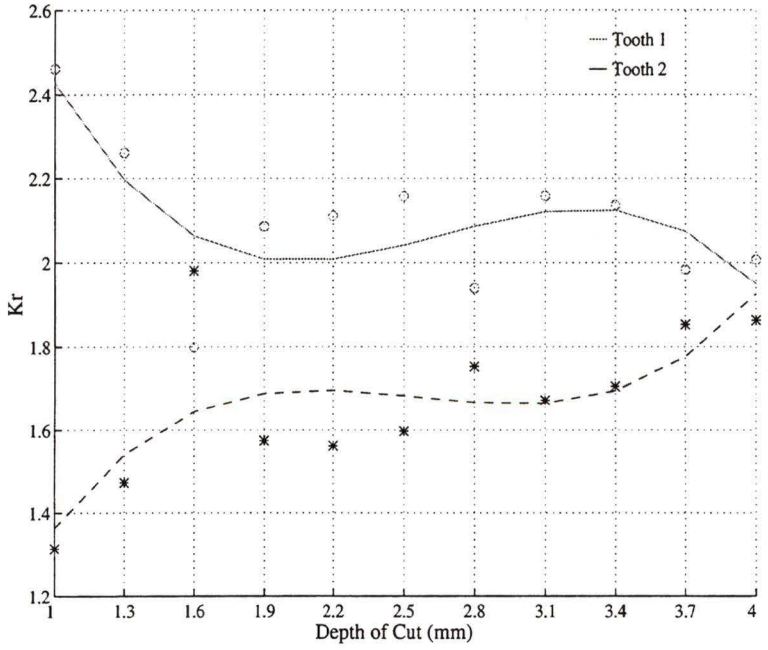

Figure C.6: Average K_r as a function of the axial depth of cut.

Appendix D

Tabulated Differences In Between Test and Prediction Values

Experimental results have shown that the differences between measured cutting force and its predicted value range from -5.22 to 20.88 percent for the old tool and from -12.96 to 3.57 percent for the new cutter. Illustrations of these results were presented in Chapter 5; remaining that numerical values to be assembled in Tables D.1 and D.2.

Note for Table D.1: All tests were carried out at a cutting speed of 30 m/min with the exception of test 8, which was conducted at a speed of 45 m/min.

Note for Table D.2: All tests were carried out at a cutting speed of 30 m/min with the exception of test 7, which was conducted at a speed of 40 m/min.

Test	d (mm)	s_t (mm/rev/tooth)	K_t	K_r	F_t	F_r	F
1	1	.2	14.30	24.46	14.30	36.22	20.88
2	1	.4	11.73	30.13	11.73	38.57	18.70
3	1	.64	7.48	21.71	7.48	27.71	10.98
4	2	.3	5.32	8.78	5.32	14.11	8.10
5	2	.5	6.31	12.13	6.31	17.70	9.39
6	2.5	.2	5.37	5.23	5.37	11.14	7.45
7	2.5	.45	7.11	11.57	7.11	17.92	10.56
8	2.5	.45	-0.30	7.69	-0.30	7.87	2.52
9	3	.33	2.58	0	2.58	2.91	2.69
10	3	.4	3.98	5.13	3.98	9.04	5.70
11	4	.2	-2.47	-7.84	-2.47	-9.30	-5.22

Table D.1: Percentile differences between test and prediction values for the old cutter.

Test	d (mm)	s_t (mm/rev/tooth)	K_t	K_r	F_t	F_r	F
1	1	.2	-0.26	5.88	-0.26	7.03	1.44
2	1	.4	2.38	6.27	2.38	8.86	3.57
3	1	.5	1.12	3.15	1.12	4.34	1.60
4	1	.64	-1.08	-4.99	-1.08	-5.92	-1.65
5	2	.3	-4	1.96	-4	-1.39	-3.24
6	2	.5	-0.36	6.84	-0.36	6.53	1.38
7	2	.3	-4.58	1.70	-4.58	-1.90	-3.74
8	2.5	.2	-7.71	0.66	-7.71	-6.02	-7.13
9	2.5	.45	-2.43	7.19	-2.43	4.99	-0.18
10	3	.33	-5.96	1.09	-5.96	-4.44	-5.44
11	3	.4	-2.58	4.27	-2.58	1.93	-1.06
12	4	.2	-10.60	-6.38	-10.60	-16.38	-12.96
13	4	.3	-7.47	-3.57	-7.47	-10.56	-8.70

Table D.2: Percentile differences between test and prediction values for the new cutter.

VITA

Surname: Pop Given Names: Sorin Ion

Educational Institutions Attended:

University of Victoria	1993-96
Technical University of Timisoara	1986-91

Degrees Awarded:

Diploma in Engineering	Tech. Univ. of Timisoara	1991

Honours and Awards:

Graduate Teaching Fellowship, University of Victoria	1995-96
Research Assistantship, University of Victoria	1994-96
University of Victoria Fellowship	1993-94
Advanced Systems Institute Scholarship	1993
Overseas Research Scholarship, Cambridge University	1992-93
Honour Scholarship, Technical University of Timisoara	1989-91
First Prize at Student Symposium, Technical University of Timisoara	1989
Special Prize at Student Symposium, Technical University of Timisoara	1988
First Prize at *Traian Lalescu* Design Competition, Technical University of Timisoara	1987

Publications:

Author

Drive Design for a Machining Centre, Diploma in Engineering Thesis	1991
Automated Designing of Belt Driven Transmissions, Proceedings Student Symposium	1989
Solution for Determining The Geometrical Characteristics of Cross-Sections, Proceedings Student Symposium	1988

Co-Author

Cutting Edge Geometry for Milling Cutters, Scientific Bulletin, Tech U Timisoara	1991
Determination of Knives Profile for Hob Milling Cutter Relief with Circular Setting Surface, Scientific Bulletin, Tech U Timisoara	1991
Technological Problems Encountered at the Installation of Abrasive Tools for Hob Type Milling Cutter Relieving, Scientific Bulletin, Tech U Timisoara	1989

Unpublished four papers

PARTIAL COPYRIGHT LICENSE

I hereby grant the right to lend my thesis to users of the University of Victoria Library, and to make single copies only for such users or in response to a request from the Library of any other university, or similar institution, on its behalf or for one of its users. I further agree that permission for extensive copying of this thesis for scholarly purposes may be granted by me or a member of the University designated by me. It is understood that copying or publication of this thesis for financial gain shall not be allowed without my written permission.

Title of Thesis:

Machining Process Model for Intelligent Rough Machining of Sculptured Parts

Auth[redacted]

Sorin Ion Pop

May 27, 1996

Date